AD-A102 746 TECHNION - ISRAEL INST OF TECH HAIFA DEPT OF MATERIA--ETC F/G 11/6
SUPERSATURATED ALUMINUM ALLOY POWDERS.(U)
JUL 81 D SHECHTMAN AFOSR-80-0224

UNCLASSIFIED EOARD-TR-81-8 NL

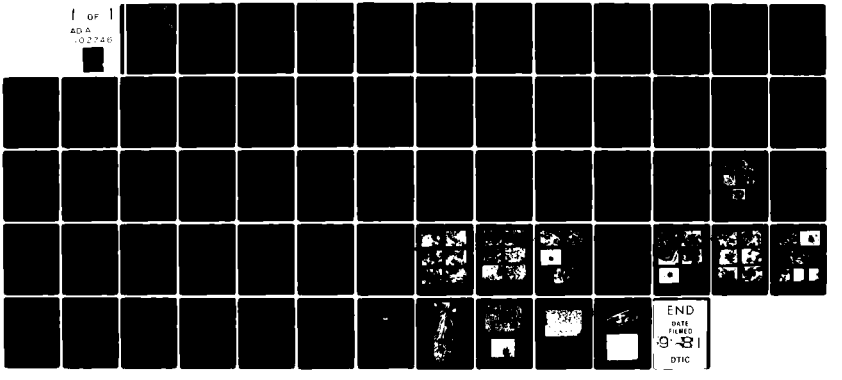

EOARD-TR-81-8

LEVEL II

(2)

Grant Number AFOSR - 80 - 0224

SUPERSATURATED ALUMINUM ALLOY POWDERS

AD A102746

Dan Shechtman

Dept. of Materials Eng.
Technion
Haifa, Israel

DTIC
ELECTE
AUG 11 1981
D

July 15, 1981

Final Scientific Report, 1 July 1980 - 30 June 1981

Approved for public release; distribution unlimited

DTIC FILE COPY

Prepared for

United States Air Force
Air Force Office of Scientific Research
Bolling AFB DC 20332

and

European Office of Aerospace Research and Development
London, England

REPORT DOCUMENTATION PAGE		READ INSTRUCTIONS BEFORE COMPLETING FORM
1. Report Number EOARD-TR-81-8	2. Govt Accession No. AD-A102746	3. Recipient's Catalog Number
4. Title (and Subtitle) Supersaturated Aluminum Alloy Powders		5. Type of Report & Period Covered Final Scientific Report July 1980 - June 1981
		6. Performing Org. Report Number
7. Author(s) Dan Shechtman		8. Contract or Grant Number AFOSR-80-0224
9. Performing Organization Name and Address Dan Shechtman Dept. of Materials Eng. Technion, Haifa, Israel		10. Program Element, Project, Task Area & Work Unit Numbers 61102F 2303/D1
11. Controlling Office Name and Address European Office of Aerospace Research and Development/LNM Box 14 FPO New York 09510		12. Report Date 15 July 1981
		13. Number of Pages 61
14. Monitoring Agency Name and Address		15.

16. & 17. Distribution Statement

Approved for public release; distribution unlimited.

18. Supplementary Notes

Prepared in cooperation with (Mrs.) R. Yearim

19. Key Words

Aluminum alloy powders, supersaturation, electron-microscopy, microstructure mechanical properties, elevated temperatures

20. Abstract: Four aluminum alloys, designed for use at elevated temperatures, supersaturated with iron, chromium and other elements were studied. The starting materials were alloy powders made by the RSR (PcWA) Process, and extrusion bars were made from the four alloys. The microstructure of the extrusion bars as well as that of the as-received powders were studied by transmission electron microscopy. The thermal stability of the alloys and their mechanical properties were tested at various temperatures up to 482°C (900°F). Analysis of the solidification process of the rapidly solidified powder is presented.

FORM 1473

EOARD-TR-81-8

This report has been reviewed by the EOARD Information Office and is releasable to the National Technical Information Service (NTIS). At NTIS it will be releasable to the general public, including foreign nations.

This technical report has been reviewed and is approved for publication.

JOHN O. GOWAN
Major, USAF
Chief, Materials & Chemistry

GORDON L. HERMANN
Lt Colonel, USAF
Deputy Commander

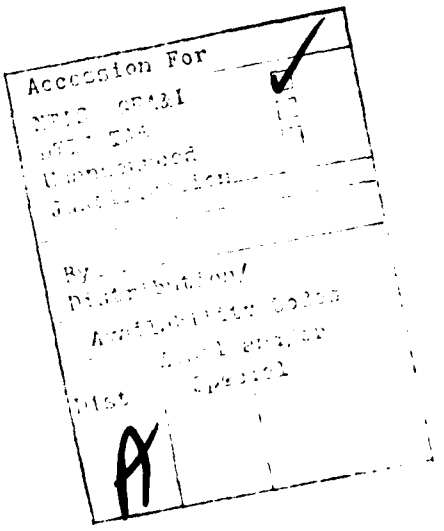

Acknowledgement.

I wish to express my gratitude to L.R. Bidwell and W.M. Griffith who helped the research with their experience. To A.M. Adair and the Westinghouse group at AFWAL for the compaction and extrusion of the powders and to many of my colleagues at the AFWAL and at the Technion who showed interest in this study.

Figure Captions

1. The tensile and creep specimen.
2. The shape of the powders (SEM) (a)(b)(c) and (d) are alloys 1,2,3 and 4 respectively. (e) The impact of a molten drop on a particle.
3. Hardness vs. soaking time at 231°C.
4. Hardness vs. soaking time at 400°C.
5. Hardness vs. soaking time at 482°C.
6. X-ray diffraction - as extruded.
7. X-ray diffraction - 100 hours at 482°C.
8. Al-Fe-Cr, 425°C isotherm.
9. X-ray diffraction relative intensities - as extruded
10. X-ray diffraction relative intensities - 100 hours at 482°C.
11. Transverse (a c e g) and longitudinal (b d f h) cross sections of alloys 1, 2, 3 and 4 respectively. As extruded, optical microscopy x 600
12. Large precipitates at grain boundaries (a b c d) alloys 4, 2, 3, 3 respectively. (e, f) - areas free of precipitates alloys 3 and 4 respectively.
13. Various shapes and sizes of precipitates. a, b and c alloys 2, 3 and 1 respectively. (d) (e) - homogeneous distribution of small needle-like precipitates at grain boundaries and in the grains (alloys 1 and 2, as extruded, respectively). (f) - globular precipitates at grain boundaries and needle like in the grains (alloy 1 as extruded).
14. (a),(b) equiaxed grains, alloy 1 as extruded
    (c),(d) diffraction pattern and its analysis (zone axis $[\bar{1}11]$).
    (e) Thickness fringes taken in two beam conditions analyzed ag g=[220].
15. Superimposed stereographic projections of the precipitate AL_6Fe in the aluminum matrix.
16. (a),(b) Needle-like precipitates, alloys 3, 100h at 482°C.
    (c),(d) B.F and D.F. images of large needle-like precipitate
    (e),(f) SAD and its analysis identifies precipitate at (c) and (d) as Al_3Fe.

17. (a),(b) Inhomogeneous distribution of precipitates into groups according to shape and size. Alloys 2 and 3 respectively, 100 hours at 482 C.
(c),(d) Large spheroidal Al_6Fe precipitates at grain boundaries.
(e) depleted zone, alloy 2, 100h, 482°C.
(f) Equiaxed grains, alloy 1, 100 h, 482°C.

18. (a) Precipitates distribution, alloy 1, 100 h, 482°C.
(b) SAD from a coarse needle-like θ Al_3Fe precipitates, streaks and satellites appear in the pattern.
(c) The diffracting precipitate (marked A).
(d) STEM image (B.F.) of precipitates (Note groups A, B, C)
(e) X-ray mapping of iron (Fe), concentrated at the precipitates (Note concentration at points A, B, C in (e)).
(f) X-ray mapping of chromium (Cr.).

19. Stress-strain curves of alloy 1.

20. Stress strain curves of alloy 2.

21. Stress strain curves of alloy 3.

22. Steady state creep rate vs. creep strain of the three alloys at 222°C.

23. Steady state creep rate vs. creep strain of the three alloys at 338°C.

A1 The pressure cell.

A2 Solidification in one powder particle starts at the interior near the center. (TEM, Alloy 2, as received).

A3 Nucleation centers near the surface of the particle. Large cells indicate slow propagation of solidification front.

A4 SAD from a particle. The rings diffract from the cell boundaries.

A5 Dark field image taken from a section of the diffracting ring.

A6 X-ray image of iron (Fe) shows concentration of this element on the cell boundaries.

Abstract

Four aluminum alloys, designed for use at elevated temperatures, supersaturated with iron, chromium and other elements: Ti, V, Zr, were studied. The starting materials were alloy powders made by the RSR (Rapid Solidification Rate) centrifugal atomization process ($\sim 10^6 [\frac{C}{sec}]$) developed by Pratt and Whitney Aircraft and extrusion bars were made from the four powders. The as extruded microstructure and the microstructure of the annealed alloys at 482°C (900°F) were investigated by optical and transmission electron microscopy, and by X-ray diffraction. The microstructure included equiaxed grains of aluminum matrix and two types of precipitates, namely: θ-$Al_3(Fe,Cr)$, and $Al_6(Fe,Cr)$-- which is a metastable phase. The precipitates were different in their shape, size, distribution and location within the grains. The thermal stability of the four alloys was investigated by hardness measurements, following annealing at various temperatures: 230 C (450°F), 400°C (750°F), 482°C (900°F) (1-100 soaking hours at each temperature). The alloy structures were found to be stable up to 400 C (750°F). Tensile properties of the alloys were investigated at room temperature, 232°C (450°F) and 332°C (630°F).

1. Introduction

The improved strength at elevated temperatures has been a goal in aluminum alloy development for a long time [1]. A microstructure containing a dispersion of an insoluble constituent in the alloy is the most useful for attaining high strength and good structural stability at elevated temperatures [2]. In the last 35 years hardened aluminum alloys have been extensively used at the aircraft industry in the U.S. [1], thanks to their relatively low price and their high specific strength at ambient temperatures. The thermal stability of high strength aluminum alloys in use today is rather poor. The strength decreases rapidly with increasing temperature and with increasing

soaking time at temperatures above (170°÷180°C), and thus the supersonic aircraft industry (2.7÷3.3 mach) had to replace aluminum alloys with more exotic and expensive materisls, namely titanium alloys, to achieve good performance of parts and structures designed to be exposed to elevated temperatures. The use of thermally stable aluminum alloys with increased strength at elevated temperatures is expected to perform properly at elevated temperatures with the advantage of lower cost and lower components weight.

The powder atomization technology development at the ALCOA laboratories in U.S. [1], [2] and the splat-cooling technology development is expected to push aluminum alloys performance to limits previously unknown.

In various research projects transition metal alloying additives were used. These elements have [2]:

1. High solubility in molten aluminum.
2. Low solid-solubility in aluminum.
3. A low diffusion rate in aluminum.
4. A high solidus temperature and a low liquidus temperature.
5. A tendency to form stable precipitates at elevated temperature.

These qualities are needed in order to retain the structural stability of the alloy at service temperatures by the internal introduction of hard and stable fine dispersion of intermetallic compounds. A high degree of supersaturation can be achieved by rapid solidification ($\sim 10^5 [\frac{°C}{sec}]$) of such alloys. Sequent operations following compaction and fabrication enables controlled precipitation in solid state of the intermetallic phases, which attain high strength and good structural stability at elevated temperatures [2].

Iron and chromium, among other elements, meet the requirements listed anove and, furthermore, when combined with aluminum they form intermetallic

compounds of fairly low density. This, appreciable amounts of alloying elements may be added without a prohibitive increase in the density of the final product [2]. Precipitation processes and some of the mechanical properties of certain aluminum alloys containing mainly, Ti, Zr, Mn, Cr, Ni, V, Fe were investigated in the past [2], [3], [4], [5], [6], [7]. The main encouraging results were high yield and tensile strengths and the retention of strength after exposure to relatively high temperatures.

The goal of this work was to investigate systematically four aluminum alloys, supersaturated with iron and chromium and with other elements (Ti, V, Zr). The compositions of the four alloys are (in weight percentage):

1. Al-7Fe-1.0 Cr-0.2 (V,Ti,Zr)
2. Al-7Fe-1.0 Cr
3. Al-7Fe-0.5 Cr
4. Al-7Fe-1.5 Cr

Powders of the four alloys were generated by the RSR (Rapid Solidification Rate) centrifugal atomization process ($\sim 10^6 [\frac{°C}{sec}]$), developed by Pratt and Whitney Aircraft. Extrusion bars were made from the four powders. The extrusions (and the powders) were supplied by the U.S. Air-Force (AFWAL MLLS WPAFB).

The study was aimed at:

1. Characterization of the four powders by Scanning-Electron Microscopy (SEM).
2. Study of the thermal stability of the alloys at the temperature range: 232-482°C (450-900°F).
3. Study of the tensile properties of the alloys at room temperature and at elevated temperatures: 232°C (450°F), 332°C (650°F).
4. Identification of the phases present in the extrusion bars by X-ray diffraction and by electron-diffraction.

5 Microstructural investigation by optical and transmission electron microscopy (TEM) and STEM of extruded specimens of the four alloys in as-extruded condition and following annealing for 100 hours at 482°C (900°F).

2. Experimental Procedures

2.1 Material preparation

2.1.1. Splat-cooling and powder production

The four supersaturated aluminum alloy powders were generated by the RSR (Rapid Solidification Rate) centrifugal atomization process, developed by Pratt and Whitney Aircraft. In this technique a vacuum induction melt is poured through a small nozzle onto a rapidly rotating disc, the alloy is fragmented and ejected at speeds of 40-100 [m/sec] and then atomized and rapidly quenched by high velocity helium jets. (Solidification rate: 10^5-10^6 $[\frac{°C}{sec}]$) [8]. A quantity of about 1 kg was prepared from each alloy.

2.1.2. Compaction and extrusion

The four powders were extruded at the U.S. Air-Force Materials laboratories AFML/MLLM by the following steps: (a) compaction: The powders were partially consolidated hydrostatically in a rubber bladder to a cylinder which size matched the dimensions of a can (made of Al-6061 alloy)*. (b) degassing: The compacted cylinders were inserted into cans which were then sealed except for an evacuation tube opening. The cans were evacuated and heated to 482°C (900°F) for degassing. The degassing temperature was designed to reach the highest expected extrusion temperature in order to eliminate hydrogen blistering in the final extrusion product. The degassing

---

* During this process one of the bladders tore off and the powder Al-7Fe-1.5 Cr was contaminated with oil. Nevertheless, this powder was extruded later on like the other powders.

process ended when no signs of gas were observed on the pressure gauge (about five hours). The tubes were then sealed and the cans were ready for extrusion. (c) extrusion: Extrusion of the billets were made at a ratio of 39.3 to 1. The die was preheated to 500°F and the billet to 400°C (750°F) in an air-furnace for about two hours. During the extrusion process the temperature of the extrusion was expected to reach 482°C (900°F). The extruded bars had a length of about 150" and were 1/2" in diameter.

Specimens for thermal treatments, hardness-tests, optical and electron microscopy and X-ray diffraction were taken from the central part of each extrusion bar.

2.2 Determination of the microstructure

2.2.1. Phase Identification by X-ray diffraction

X-ray diffraction was used to identify phases which are present in the four extrusion bars, at the as extruded condition and after annealing for 100 hours at 482°C (900°F). The diffraction was carried out in a Phillips vertical diffractometer using CuKα radiation and a monochromator.

Powder specimens were made from the central part of each extrusion bar to avoid texture effect on the diffraction peak intensities. Other powders were made from heat treated bars. The heat treatment was carried out in sealed stainless steel bags, in an air furnace. These heat treated bars were also studied later on by optical and transmission electron microscopy.

2.2.2. Optical Metallography and Electron Microscopy

Vertical and longitudinal metallographic specimens were prepared from the central part of each extrusion bar, at the as-extruded condition and after annealing at 482°C (900°F) for 100 hours in an air-furnace. The same specimens were also studied by transmission electron microscopy.

Transmission-electron microscopy was carried out in a Jeol 100-B TEM and in a Jeol 100-C-X STEM with an accelerating voltage of 100 kV. An X-ray mapping was done for the elements: Iron and Chromium in a TEM specimen. The mapping was carried out by an energy dispersive system (EDS) attached to the STEM unit. The EDS system is of the type Elscint Proxan III, with a solid-state Si(Li) X-ray detector. TEM specimens, 3 mm in diameter were prepared in a two stage electropolishing process:

(a) Stage I : This polishing and pre-thinning stage is done in a jet apparatus built for the project. The electrolyte found best for electropolishing the specimens is:

950 ml - CH_3OH - methanol abs.
50 ml - $HClO_4$ - perchloric acid
15 ml - HNO_3 - nitric acid

Conditions of the electropolishing process are as follows:

Jet diameter - 1.5 mm
D.C. voltage - 100 volts
room temperature.

Distance between cathode (austenitic stainless steel) and specimen - 6 mm. The disc is mounted on a stainless steel grid and a minimum jet stream without breaking into drops is used (gravitational flow). Both sides are thus electropolished in a period of about 30 seconds.

When the thickness at the center of the concaved disc reaches 50μ the process is stopped and the specimen is subjected to the second electropolishing stage.

(b) Stage II : Electropolishing is done using the same electrolyte as in Stage I and the window technique is used. Other conditions are as follows:

Current density - 0.15 A/cm^2

D.C. voltage - 10÷15 volts

Temperature - -40°C or less

Cathode - austenitic stainless steel

Cooling liquid - water + methanol (Tech) 10%.

This stage is carried out slowly to ensure proper inspection of the first stage of performation and even polishing of both surfaces of the disc.

Good thin foils for TEM study are obtained after 15÷30 min.

2.3 Determination of Mechanical Properties

2.3.1. Thermal stability measurements (hardness measurements).

Specimens for thermal treatments were sliced from the central part of each extrusion bar, and the aluminum shell around the bar removed. The purpose of the thermal treatments was to study the thermal stability of the alloys at elevated temperatures : 232°C (450°F), 400°C (750°C), 482°C (900°F). (1,5,30,100 soaking hours at each temperature). The specimens were inserted into stainless steel bags to eliminate oxidation, and thermal treatments were carried out in an air furnace. Temperature measurements were made using Chromel-Alumel thermocouple.

The specimens were pre-heated to the various temperatures the indicated time periods and then air-cooled. Rockwell hardness measurements were carried out on each specimen as well as on preheated specimens of the four alloys.

2.3.2. Tensile Tests

Tensile tests on specimens made of the extrusion bars were carried out in an Instron testing machine. The cross head velocity used was 0.5 mm/min and alloys number 1, 2 and 3 were tested.*
The shape of the tensile specimen is given in Fig.1.

Test temperatures used were:

a) 25 C

b) 232°C (450°F)

c) 332°C (630°F)

2.3.3. Creep Tests

Specimens of the alloys 1, 2 and 3 which shape was identical to the tensile test specimens were tested in creep at the temperatures 222°C and 338 C (432 and 640°F). Each specimen was tested until a steady state creep rate ($\dot{\varepsilon}_{ss1}$) was achieved. After a few hours in this rate, the stress on the specimen was increased and a second steady state creep rate was obtained ($\dot{\varepsilon}_{ss2}$). The specimen was then tested until final failure.

3. Results

3.1. Shape of powders

The shape of the four powders as observed by scanning electron microscopy is given in Fig.2 (a - d). The majority of the particles, irrespective of size, have a distinctly rounded and frequently near perfect spheroidal shape. A small proportion of the particles have a lengthened shape and flake-like morphology. Particle size varied in the range : 10:100 [μm] and

* Alloy # 4 that was contaminated during the compaction stage was not tested.

some particle aggregation can be observed. Another phenomenon, shown in Fig. 2e is a collision involving a moleten droplet onto a previously solidified cold particle. This phenomenon has been demonstrated and discussed in the past [9].

3.2. Hardness data for the evaluation of thermal stability.

The room temperature hardness measurements of the four alloys as function of soaking time at various temperatures are given in Figs. 3, 4 and 5. The temperature uses were: 231°C, 400°C and 482°C (450, 750 and 900 degrees F, respectively). At the soaking temperature of 231°C (Fig.) the hardness values of the four alloys are unchanged up to an annealing time of 100 hours. This indicates a rather high degree of thermal stability. The hardest alloy is number 1 followed by 4, 2 and 3 in decreasing order. This order is retained through all the soaking temperature and times. The thermal stability is maintained for 100 hours at the soaking temperature of 400°C as well (Fig. 4), however at 482°C there is a sharp decrease in hardness after few hours, depending on the alloy (alloy 1 being still the best). This decrease is typically 20 per cent in 100 hours (except for alloy # 2, for unexplained reasons)(Fig. 5).

3.3. X-ray diffraction

Phases identification in the four alloys was done by X-ray diffractometry. The analysis was done in the as-extruded condition and after annealing for 100 hours at 482°C (900°F). The diffraction intensity results are produced in Figs: 6 (as extruded) and (after annealing).

The phases which were identified in the four alloys in the as-extruded condition as well as after annealing are:

1. Aluminum matrix
2. Al_6Fe
3. Al_3Fe

The last two phases contain probably chromium in solid solution, since no chromium-base intermetallic compound was detected. The minor amounts (0.2%) of the other additional elements in alloy 1, namely Ti, Zr and V, are also expected to be in solid solution.

An extrapolation of Al-Fe-Cr, 425°C, isotherm (Fig. 8) indicates that there is no precipitation of Al_7Cr phase in alloys containing less than 1.5 w/o Cr. Alloy 4, with 1.5 w/o Cr is on the threshold of precipitation.

3.3.1. Phase identification

α-Al phase was identified according to ASTM card : 4-0787, the Al_3Fe phase according to ASTM card 2-1213. There is a little information available however regarding the Al_6Fe metastable phase. This phase is isomorphous with the equilibrium phase Al_6Mn [10] (ASTM card : 6-665, both phases are orthorhombic): d-values and bragg angles were calculated for the Al_6Fe phase, and Schemes of X-ray diffraction of the alloys are shown in Figs: 9 and 10 with a reference graph of the phases according to ASTM cards and calculation. The relative intensities in the X-ray diffraction schemes are normalized.

The relative quantities of the phases Al_3Fe and Al_6Fe, as can be roughly estimated from the X-ray intensities, are different in each alloy. Alloy 1 contains a higher quantity of Al_3Fe and the other alloys contain a larger amount of Al_6Fe. The annealing procedure (100 hours at 452°C) lowers the amount of Al_6Fe in all the alloys and the amount of Al_3Fe is increased.

3.4. Optical Metallography

Optical micrographs of vertical and longitudinal sections of the four alloys are shown in Fig. 11. A banded structure is observed along the extrusion direction in alloys containing the elements Fe and Cr only alloys - 2, 3, 4). Alloy 1, containing also Ti, V, Zr, presents a more homogenic microstructure.

3.5. Microstructural investigation by transmission electron microscopy (TEM).

3.5.1. The microstructure in the as-extruded conditions

The microstructure of the four alloys, in the as-extruded condition, consists of equiaxed grains of α-Al matrix and of two kinds of precipitates. These two kinds differ in shape as follows:

(a) Large, spheroidal precipitates: that tend to form along the α aluminum grain boundaries.

(b) Smaller, needle-like precipitates.

Measurements of precipitate sizes were carried out on 10 micrographs from each alloy, and standard deviation calculated. (Table 1 and Fig. 12, a, b, c, d) A few areas, consisting of large grains, almost clean of precipitates were detected at the location of the large-precipitate groups. (Fig. 12, e, f). The needle-like precipitates distribution was found to be rather homogeneous (Fig. 13) The regions, in all the four alloys, consisting of equiaxed grains were found to contain mainly large precipitates (Fig. 14, a, b). The smaller grains, however, contain a larger quantity of smaller precipitates (Fig. 13, d, e). Alloy 1, is distinguished from the other alloys by having a more homogeneous precipitate distribution (Fig. 13, f, e): No distinct grouping of precipitates was detected in this alloy and only few areas, containing large precipitates were detected. The TEM specimen thickness, necessary for precipitation density measurements, was determined using thickness

fringes. Twenty micrographs were used for each alloy for the density measurements. Mean and standard deviation were calculated and are presented in Table 1.

Grain size measurements were carried out on 10 micrographs of each alloy and the results are presented in Table 1.

Diffraction patterns of several orientations were obtained from the large precipitates, which were identified as the metastable phase: Al_6Fe. An example is presented on Fig. 14, a, b, c. In order to determine orientation relationships between the Al_6Fe phase precipitates and α-Al matrix, a diffraction pattern containing the precipitate and α-Al matrix reflections was taken and zone-axes of the two phases were identified. An example of superimposed stereographic projections of the precipitate* and matrix related to their zone-axis are shown on Fig. 15. No orientation relationships were found between the Al_6Fe precipitate and matrix. Diffraction patterns from the needle-like precipitates, identified as the equilibrium phase: θ-Al_3Fe, is shown in Fig. 16, c, d, e, f.

3.5.2. The microstructure after annealing

Bright field images reveal, in general, coarser structure after 100 soaking hours at 482°C (900°F). Precipitate grouping according to size and shape exists, except for alloy #1 (Al_6Fe precipitates). These, located at grain-boundaries, tend to be more spheroidal in shape than in the as-extruded structure (Fig. 17) and there is an increase in precipitate-size (see Table 2). The number of the larger precipitates increases and the small precipitates dissolve, thus more areas isolated of precipitates exist (Fig. 17, e, f). There is also a slight increase in the size of the

* The stereographic projections were computer drawn according to a computer programme programmed by Prof. I. Blech of the Dept. of Mat. Eng. at the Technion

θ-Al_3Fe, needle-like precipitates (Fig. 16 a) and among them there are rather large ones (Fig. 16c). There is also an increase in grain-size (see Table 2) Fig. 17, c, e, f. We have also observed that grains containing small precipitates tend to grow less than those which are clean from Al_3Fe precipitates.

Alloy #1 (Al-7Fe-1.0Cr-0.2 (Ti, V, Zr) has a uniform grain-size which matches the size of the larger grains in the other alloys (Table 2 and Fig. 17f). In this alloy most of the precipitates are of the Al_3Fe type (needle-like in shape) and very few are of the spheroidal type Al_6Fe (Fig. 18a). A small portion of the needle-like precipitates are coarsened due to the annealing treatment Fig. 18c . These coarsened precipitates seem to contain (according to bright-field images), planar faults, running along the precipitate length or width. Streaks and satellites appear in diffraction patterns taken from these precipitates. Fig. 18 b, c.

3.5.3. X-ray mapping

X-ray mapping was carried out on a specimen of alloy #2 (Al-7Fe-1.0Cr), after annealing (100 soaling hours at 482°C) for the elements: iron (Fe) and chromium (Cr.). A S.T.E.M. image of the precipitates is shown in Fig. 18 d. It can be clearly seen that most of the iron is concentrated in the precipitates (Fig. 18 e), X-ray mapping immage for the chromium is not very clear, but one can see that chromium, too, concentrates mostly in the precipitate (Fig. 18 f). In conclusion, the precipitates of metastable phase, Al_6Fe and of the equilibrium phase, θ-Al_3Fe contain Fe and Cr, namely $Al_6(Fe, Cr)$, $Al_3(Fe, Cr)$.

3.5.4. Room temperature and elevated temperature tensile properties

Room temperature and elevated temperature (232°C, 322°C) tensile properties are presented in Figs. 19, 20, 21 respectively, for tensile specimens of three alloys:

a. Alloy # 1 Al-7Fe-1.0 Cr-0.2 (Ti,V,Zr)

b. Alloy # 2 Al-7Fe-1.0 Cr

c. Alloy # 3 Al-7Fe-0.5 Cr.

In general, as expected, there is a decrease in strength with increase in testing temperature. Alloy 1 has the highest yield and tensile strengths at all test temperatures. Alloy 2 has a lower yield and UTS stresses but is slightly better than alloy 3 (Table 3). The elongation to fracture at room temperature is almost identical in all the alloys. At 232°C (450°F) the elongation to fracture decreases in all the alloys. The greatest decrease occurs in alloy 1 and the smallest in alloy 2. At 332°C (630°F) the elongation to fracture increases in alloys 1 and 2, but the elongation of alloy 3 decreases still further. The measurements of the reduction of area reflect the same behavior. (See Table 3). At the elevated testing temperatures alloy 1 has the lowest elongation to fracture and alloy 2 has the highest one.

2.5.5. Creep tests results

The dependence of the steady state creep rate on the load applied is presented in Figs. (22) and (23). The stress sensitivity factor (the slope of the parallel lines is n=8 for T=222°C and n=11 for T=338°C. The activation energy can be estimated from these data, even though the number of tests is limited, using the equation:

$$Q = -R \frac{\ln \dot{\varepsilon}(T1) - \ln \dot{\varepsilon}(T2)}{\frac{1}{T1} - \frac{1}{T2}}$$

The activation energy of alloy 1 is Q=40 Kcal/mole.

Discussion

The temperature regime to which the alloy powders were exposed during the compaction process have a great influence on the microstructure and thus the properties obtained thereafter. The degassing process done at 482°C (900°F) during 5 hours was followed by air cooling of the sealed cans. The extrusion process was preceded by the heating of the canned powders to 400°C (750°F) for two hours, and during the extrusion process the temperatures are expected to rise to about 482°C (900°F) in portions of the extrusion cross section.

This rather prolonged exposure to temperature causes the precipitation of the $Al_3(Fe,Cr)$ of the $Al_6(Fe,Cr)$ in rather uncontrolled conditions. It is assumed, therefore, that better properties can be obtained in a compaction process that will avoid the exposure to high temperatures. Controlled thermal treatment will then be employed to generate optimum precipitation size and distribution. The technique that could be employed for cold compaction of this powder will be discussed later on.

The main characteristics of the alloys' microstructures were demonstrated before and can be summarized as follows:

a. All the alloys, except alloy #1 exhibit banded structure which consists of elongated bands of varying precipitate concentrations. This microstructure is observed by optical microscopy and confirmed by transmission electron microscopy. Alloy #1 is more homogeneous and no such bands could be detected in it.

b. All the alloys have small grain size, of the order of 1 to 3 μm, and the two kinds of precipitates are located in two typical sites. The $Al_6(Fe,Cr)$

are found only along the grain boundaries. The $Al_6(Fe,Cr)$ which are generally globular in shape are rather large (0.15:0.52 μm) and their main contribution to the mechanical properties is in apparently the stabilization of grain size, since the grains were found to grow very little after prolonged annealing. The other kind of precipitates, namely the $Al_3(Fe,Cr)$ is distributed evenly within the grains, and contribute to the mechanical properties by serving as incoherent dispersoids to block dislocation movement. These needle like precipitates are 0.1:0.3 μm in length and have no distinct orientation relationship with the aluminum matrix.

The iron which is a major constituent of the alloys is thus divided between the two kinds of precipitates. Previous works [11] [12] [13] mention that the stable Al_3Fe is retained following heat treatments while the Al_6Fe is transformed, apparently to Al_3Fe, in alloys that do not contain chromium. The alloys, numbers 2,3,4 in our study, retain the $Al_6(Fe,Cr)$ after exposure to temperatures within the range reported by other investigators [11] [12] [13] This can mean that the chromium additions stabilize the $Al_6(Fe,Cr)$ at higher temperatures

Alloys #1 with the additives 0.2 T, 0.2 V, 0.2 Zr, contain, following exposure to temperature regimes as shown before, mainly precipitates of type $Al_3(Fe,Cr)$. The difference in composition between this alloy and alloy #2 is only in these additives, while the other constituents are the same, namely 7% Fe and 1% Cr. The fact that alloy #1 contain almost no $Al_6(Fe,Cr)$ as opposed to alloy #2 whose microstructure contains, roughly, equal amounts of $Al_3(Fe,Cr)$ and $Al_6(Fe,Cr)$ means that one or some of the Ti, V, Zr additives stabilizes the Al_3 (Fe,Cr) phase, by neutralizing the effect of the chromium.

The relative contributions of the $Al_3(Fe,Cr)$ and $Al_6(Cr,Fe)$ of the alloys can be evaluated as follows:

a. They both strengthen the alloys, $Al_6(Fe,Cr)$ by preventing grain boundary migration and $Al_3(Fe,Cr)$ by serving as a dispersoid phase to impede dislocation mobility within the grains.

b. The improved mechanical properties of alloy #1 over alloy #2 (in fact alloy #1 is better than all the other alloys at all test temperatures) may mean that the contribution of the $Al_3(Fe,Cr)$ disperoids is more important for improved mechanical properties than the $Al_6(Fe,Cr)$ phase.

A comparison between the mechanical properties of the alloys under investigation (no.1, 2 and 3) and those of several other alloys are given in Table 4 . The alloys with which the comparison is made are 2219, 2618 which are commercial high temperature aluminum alloys, and ALCOA, Al-8Fe-1.5 Cr. All three are designed to be high temperature alloys and high temperature properties are available in the literature for them. At room temperatures, our alloys are inferior in their yield strength and in their UTS. They do show, however, better ductility. At 232°C our alloys are comparable to 2219 and 2618 in their tensile properties, and except for alloy #1 which at this temperature has elongation of about 14%, the ALCOA alloy Al-8Fe-1.5 Cr is by far better in its yield strength and UTS. Its ductility is however very low. At 332°C our alloys demonstrate better yield strength and UTS than the 2219, 2618 and are comparable to the ALCOA alloy. They show however higher ductility than the ALCOA alloy. The combination of good tensile strength with relatively high ductility may indicate that the fracture toughness of our alloys is rather high. Fracture toughness, however, was not tested within the framework of this study.

Other alloys, the composition of which is close to the composition of our alloys are M-48 [2], Al-8Fe [14] [7], Al-7.6 Fe [2], Al-8Fe [14], Al-85c-1Zr [14]. We have not compared the properties of those to the properties of our alloys since their high temperature properties were not available to us.

5. Conclusions

1. Alloy #1 containing Ti, V, Zr has superior strength properties which result from the refined microstructure and stability of fine dispersion of the intermetallic particles $Al_3(Fe,Cr)$ at elevated temperatures. On the other hand ductility is inferior to our other alloys at elevated temperatures. In case further development is to be made, we recommend the composition of alloy #1 as a starting point. Properties improvement may be carried out by composition changes and by altering the processing conditions.

2. Composition changes, in order to improve alloy properties, can be done by adding larger amounts of Ti, V, Zr. This is expected to increase strength. Retention of ductility may be achieved by increasing chromium content.

3. An alteration of the processing conditions should be based on the limiting of the exposure time to high temperatures. There are several ways of consolidation that can be done at lower temperatures, i.e. cold sintering, explosive compaction and hydrostatic extrusion. Once consolidation is done at a relatively low temperature, heat treatments could be tried to obtain controlled precipitation.

Appendix A

Transmission Electron Microscopy of Metallic Powders

The powders generated for this study were studied by transmission electron microscopy. There is a special interest in the technique used for the foil preparation since it is unique in the results it produces. The technique was developed by D. Shechtman and E. Gutmanas of the dept. of materials eng. at the Technion, and was tested on alloy powders of different kinds (aluminum, titanium, copper, iron, nickel and some of their alloys). Although the technique did not work for every alloy powder tried, it was found proper for the making of TEM foils of most of the alloys tested including the ones in this study.

The techniques of TEM foil preparation known before included the embedment of the powder particles in plastic resin and subsequent slicing by a microtome. Another technique used is the embedment of the particles in an electrolitically deposited nickel foil followed by electropolishing or ion milling of the composite thus formed [15]-[18] All these techniques result in only partially satisfying results. The techniques that will be reported here is based on the cold compaction [19][20] of the powders and subsequent electropolishing of the compact.

Sample Preparation

Samples were compacted and cold sintered from powder in a piston and cylinder apparatus manufactured from sintered carbides. Specimens' dia. was 3.8 mm and working pressures, P, up to 4.0 GPA (≈ 40 kbar). A schematic drawing of the pressure cell is shown in Fig. A1. Samples with thickness varying from ~ 0.1 to ~ 0.25 mm prepared in such a pressure cell, were found strong enough for handling and for final preparation of thin foils

for TEM observations. The quality of the cold sintered samples (density and mechanical strength) depends on the pressure applied and the type of the powder, being higher for powders with high compressibility and irregular shape such as pure Al and pure Ti powders. The minimum pressure needed for sample preparation was about 1.5 GPa for pure Al, $\sim$ 2.0 GPa and for Al-7Fe-1Cr powder. Usually samples were prepared at P = 3.0 GPa. Samples prepared at P up to 4.0 GPa from rapidly solidified titanium aluminide powders - were not strong enough for handling. In this case mixture of these powders with pure Al or pure Ti matrix were prepared. The compaction of powders was performed in an Instron testing machine using low cross-head speeds ($\dot{S} < 10^{-5}$ m/min) on the final stage of compaction. Teflon spray was used for lubrication of the die walls.

Electropolishing

The electropolishing of the compacted disc can be done in any conventional way. Jet polishing produces good results except when two powders are mixed, in which case ion milling can be employed. During the electropolishing process, some care is needed in the handling of the somewhat brittle compacted discs. In most of our experiments, electropolishing was done in a two stage process. First, the disc was thinned down by a jet electrolyte at a voltage of 100 volts at room temperature. When a thickness of less than 50 μm was achieved, the foil was further thinned by the window technique, at a low temperature of -40°C, until perforation. The electrolyte used in both stages is the same reported for the preparation of foils from the bulk.

Results

Reported here are the main results of the study of the alloy Al-7Fe-1Cr. A Jeol 120 CX STEM was used and the techniques used were

standard contrast analysis, electron diffraction and X-ray analysis.

The rapidly cooled powder particles exhibit a solidification mechanism that starts, in most cases in one nucleus, near the center of the particle (Fig. A2). The cellular structure is fine in the center, representing a fast solidification rate, and coarser at the circumference of the particle, indicating a slower rate. There is a rather sharp transition zone between the two areas. When the section of a particle is near its surface, many nucleation centers are observed (rosettes). These, however, grow only very little and rather slow, as can be learned by the large cell size (Fig. A3). The powder particles are single crystals in most cases, except for the nucleation rosettes which represent a very small volume of the particle. A diffraction pattern from the particle shows not only a single crystal pattern but also a set of rings (Fig. A4). These rings diffract, as can be seen by a dark field image taken with a section of the inner ring, from the cell boundaries (Fig. A5). An X-ray image of the iron element verified that the cell boundaries are rich in iron (Fig. A6). These results indicate that the solidification mechanism of the Al-Fe-Cr alloy powders is adiabatic at the center of the particle with a very high solidification rate. At the outer part of the particle the process is non adiabatic. After reaching a certain degree of undercooling ΔT the two solidification mechanisms start, at the adiabatic stage. The very rapid solidification rate at this stage is manifested by a temperature rise which is absorbed by the undercooled aluminum. This stage terminates when the partially solidified droplet reaches the melting point (or the pseudo eutectic temperature). The undercooling value ΔT can be derived from the expresion

$$mL = MC\Delta T$$

$$\text{or } \Delta T = \frac{L}{C} \left(\frac{r}{R}\right)^3$$

where m is the mass of the solidified core

M is the entire mass of the particle

C - the specific heat

r - the radius of the inner adiabatically solidified core

R - the radius of the droplet

For r/R ~ 0.6 (as it is in the particle that is shown in Fig.) we get $\Delta T = 90°C$. This is a reasonable value for the undercooling of this system. The non-adiabatic solidification stage starts when the temperature of the droplet reaches the melting point again. At this stage the latent heat of fusion is removed by convection. The freezing time for the outer portion of the droplet is given by

$$(m-n)\ L = hA\ (T-To)\ t_{na}$$

$$\text{or } t_{na} = \frac{[1-(\frac{r}{R})^3]LR}{3h\ (T_s-T_o)} \approx 6 \times 10^{-4} \text{ sec.}$$

where : L is the latent heat of fusion

T_s - surface temperature (the melting point)

T_o - the surrounding temperature (room temperature)

t_{na} - the time for freezing (the non adiabatic stage).

Assuming that the adiabatic growth rate is limited to the sound velocity, we get that adiabatic stage may terminate after 3×10^{-9} sec, which is a few orders of magnitude shorter than the solidification time for the rest of the material.

Heat balance

The flow around the particles

The following analysis for the RSR (PεWA) Process assumes the geometrical parameters as presented in Fig.

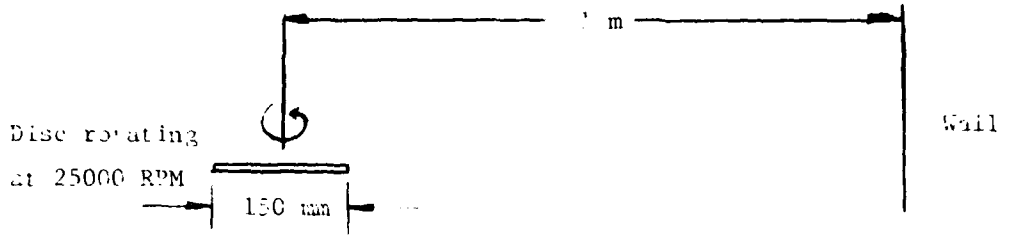

Fig. (A7)

The maximum linear velocity of the particles is given by

$$Vo = \omega r = \frac{2\pi rn}{60} r = 2.10^4 \frac{cm}{sec}$$

A more practical figure, for a droplet which strikes the disc at half distance is $Vo = 10^4 \frac{cm}{sec}$. The resistance to this movement depends on the character of the flow. Defining Reynolds number Re for this flow as

$$Re = \frac{Vo\ Ds\ Pg}{\mu g}$$

where Pg is the density of the argon gas and μg its viscosity

$2R_s = D_s$ is the diameter of the spheroid particle.

For a particle with R_s = 25 μm at the beginning of its flight we get Re = 215.

Heat flow

The heat transfer from a sphere to a flowing gas can be calculated as follows [21].

$$\frac{hDs}{kg} = 0.37\ Re^{0.6}$$

for $17 > Re > 70{,}000$

when kg is the gas heat conductivity.

Using the Reynolds number obtained before we get

$$h \cong 2500\ [F\ ft^{-2}\ h^{-1}\ °F^{-1}]$$

Other calculations show that the radiation loss can be neglected.

The time dependence of temperature distribution in a conductive spheroidal body subjected to conductive heat flow is a well known problem and its solution presented by Heisler charts [22]. When the parameter $\frac{k_s}{hR_s} > 100$ (k_s being the thermal conductivity of the spheroid), the spheroid may be treated as a body with uniform temperature. In our case $\frac{Ks}{hRS} \approx 266$ and thus uniform temperature through the volume of the sphere during cooling is assumed.

The time dependence of a uniform temperature body, cooled by heat convection is

$$\frac{T - Tf}{Ti - Tf} = e^{\frac{hAs}{\rho sCsVs}\ t}$$

when As is the area of the spheroid, ρs its density, Cs its specific heat and Vs its volume.

T is the spheroid temperature at time t, Ti its initial temperature and Tf its final temperature.

The time needed for obtaining an undercooling of about 100°C (T = 560°C) and assuming Tf = 20°C Ti = 1000°C) is $t = 10^{-3}$ sec.

Discussion

Our observations and the above mentioned considerations led us to the conclusion that the solidification of the Al-Fe-Cr powders may be divided into two stages,namely adiabatic and non-adiabatic. In the first stage, which is very fast, we assume no heat flow outside the particle. Since the heat mobility inside the particle is much faster than the heat flow through the surface; the surface is not cooler than any other point in the bulk of the droplet. The solid crystalline nucleus that starts to grow, transfers its latent heat to the bulk of the droplet and raises its temperature. We shall consider now two cases: the first, in which the nucleus is at the interior of the droplet and the second in which the nucleus is near the surface. In the first case the nucleus sees a large cold body with excellent heat mobility, which enables fast heat removal and therefore rapid solidification rate. In the second case, when solidification starts at the outer layer of the droplet.heat removal is slower since part of it is limited by the heat mobility into the surrounding gas.

Since there is a great advantage to a solid particle nucleating at the interior and since the adiabatic part of solidification is very rapid, it results in a powder particle which is mostly single crystal and in addition small crystals at the surface that cease to grow when the outcoming solidification front reaches them.

Summary

1. The powder particles contain two regions, core and periphery.

2. The regions are formed by two successive stages : adiabatic and non-adiabatic.

3. The core is formed by rapid freezing, and the latent heat does not leave the particle (because of poor heat transfer to the surrounding gas). Instead, it raises the temperature of the whole particle.

4. The periphery, which comprises about 80 per cent of the volume of the droplet, solidifies slowly, at a temperature near the melting point, and heat removal is done by convection.

5. The temperature inside the droplet is uniform throughout the bulk and there is an heterogenous nucleation that starts at the interior, and has the advantage of fast adiabatic solidification rate.

References

1. R.E. Sanders, Jr., G.J. Hildeman, D.J. Lege, "Elevated Temperature Al Alloy Development", Technical Report, AFML, 1979.
2. Towner, R.J., Metal Progress, 73 (1958) 5 p. 70.
3. Ahlborn, H. and P. Mertz, Aluminium, 47 (1971), p.671, 730.
4. Thursfield, G. et al., J. Mater. Sci. 9 (1974) p.1644.
5. Esslinger, P. and W. Wolf, Z. Wirtsch. Fertig., 60 (1965), p.449.
6. Ibid, Z. Metalkde, 57 (1966), p. 12 and 109.
7. Schuster, D.M. and M. Moss, J. Metals, 20 (1968) 10 p.63.
8. A.R. Cox, J.B. Moore, E.C. Van Reuth, Proc. 3rd Int. Symp. on Superalloys, Severn Springs, Sept. 1976.
9. B.H. Kear, P.R. Holiday, and A.R. Cox, Metallurgical Transactions, 10A, February, 1979, p.191.
10. Hollingsworth, E.H. et al. Trans AIME 224 (1962) p.188.
11. Jones, H., Mater. Sci. Eng., 5 (1969) p.1.
12. Jacobs, M.H. et al.; J. Mater. Sci., 9 (1974), p. 1131.
13. Toneje, A; Met. Trans., 2 (1971), p.437.
14. Ahlborn, H. and D. Merz, Aluminium, 50 (1974), p.583
15. H.L. Fraser and R.D. Field, TMS-AIME Fall Meeting, St. Louis, Missouri, October 1978.
16. J.S Santner, ibid
17. R.D. Field and H.L. Fraser, Met. Trans. 1978 9A 131.
18. D.G. Morris, Powder Metallurgy, 1979 4 208.
19. F.Y. Gutmanas, A. Rabinkin and M. Roitberg, Scripta Met. 1979 13 11.
20. F.Y. Gutmanas, Powder Metallurgy International, 1980 12 178.
21. McAdams, W.H , "Heat Transmission", 3rd ed. McGraw-Hill-Hill, New York, 1954.
22. Heisler, M.P , "Temperature Charts for Induction and Constant Temperature Heating", Trans AIME Vol 69, pp.227-236, 1947.

Table 1. Microstructure of the four alloys, as extruded

Alloy	Precipitates distribution	Precipitates shape	Precipitates size [μm]	Precipitates density [μm^{-3}]	Precipitates location	Grain Size [μm]
1	Homogenic. No grouping observed.	(A) $Al_6(Fe,Cr)$ 1. Elongated 2. Globular 3. Spheroidal	(A) 1. 0.52x0.45 2. 0.3 3. 0.15	(A) 1. 8 ± 3.8 2.) 3.) 7.45±3.25	(A) At the grain boundary	Grains that do not contain type B-AL_3(FeCr) precipitates 1.1±0.3
2,3 & 4	Grouping according to shape and size	(B) $Al_3(Fe,Cr)$ small needle-like precipitates	(B) 0.3x0.1	(B) 126.3±6.9	(B) In the grains	Grains containing type B-AL_3(FeCr) precipitates 0.45±0.15

Table 2: Microstructure of the four alloys, 100h at 482°C

Alloy	Precipitate distribution	Precipitate shape	Precipitate size [μm]	Precip. density [μm^{-3}]	Precipitates location	Grain size [μm]
1	Homogenic. No Grouping observed	(A) $Al_6(Fe\ Cr)$ Medium Size spheroidal (B) $Al_3(Fe\ Cr)$ small and large needle like	(A) 1. 0.65±0.13	(A) 44.3±9.5 (B) 93±16.3	(A) At grain boundaries	0.94±0.05
2, 3 & 4	Grouping according to shape and size	(A) $Al_6(Fe\ Cr)$ 1. Large spheroidal 2. Medium spheroidal (B) $Al_3(Fe\ Cr)$ Needle like	(A) 1. 0.65±0.13 2. 0.4±0.15 (B) 0.35x0.1 0.6 x0 4	(A) 1. 12.5±5.3 2. 8.5±3.5 (B) 92±17.7	(B) In the grains	Grains not containing type B $Al_3(Fe\ Cr)$ precipitates 1.3±0.45 Grains that contain type B precipitates 0.52±0.1

Table 3: Tensile properties of the three alloys at several temperatures

alloy #	Temperature [C]	UTS [MPa]	yield stress [MPa]	Elongation to fracture [%]	Reduction of area [%]
3	25	255.7	150.8	23.7	25
	232	177.7	132	18.9	23.8
	332	118.75	86.8	17.15	23.3
2	25	262.5	190.5	22.67	27.5
	232	186.5	154.8	19.9	27.5
	332	122.8	97.4	20.38	31.6
1	25	312.5	215.2	22.7	24.2
	232	220.5	191.6	13.9	20
	332	163.6	147.1	15.5	23.3

Table 4: Tensile properties of the alloys under study, and of other elevated temperature aluminum alloys.

	Alloy / Temp [°C]	#1	#2	#3	2219 T851	2618 T851	Al-8.5-1.5Cr ALCOA [1]
UTS [MPa]	25	312.5	262.5	255.7	455	441	562
Yield [MPa]		215.2	190.5	150.8	345	372	500
Elongation [%]		22.7	22.7	23.7	12	10	1
UTS [MPa]	232	220.5	186.5	177.7	221	193	401
Yield [MPa]		191.6	154.8	132	186	179	374
Elongation [%]		13.9	19.9	18.9	21	28	3
UTS [MPa]	332	163.6	122.8	118.75	65	45	184
Yield [MPa]		147.1	97.4	86.8	54	33	163
Elongation [%]		15.5	20.4	17.15	-	-	7

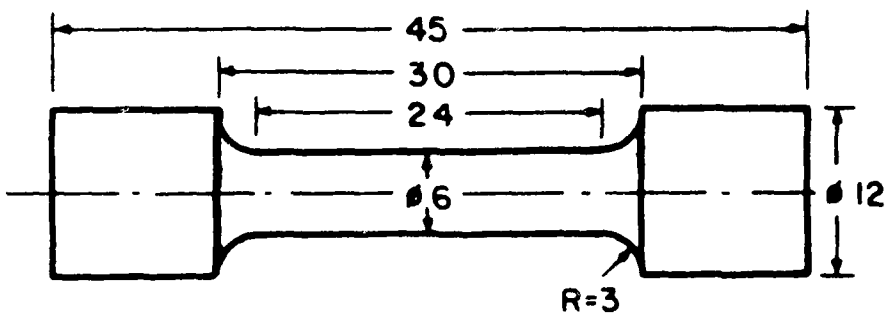

fig.1

a

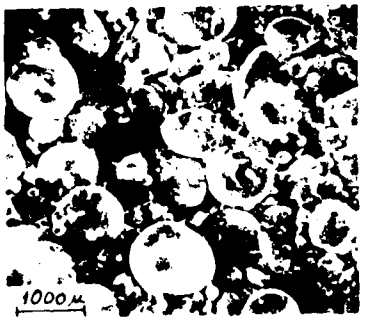

b

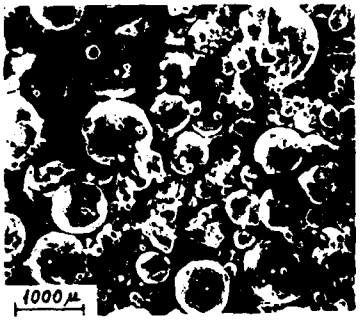

c

d

e

fig.2

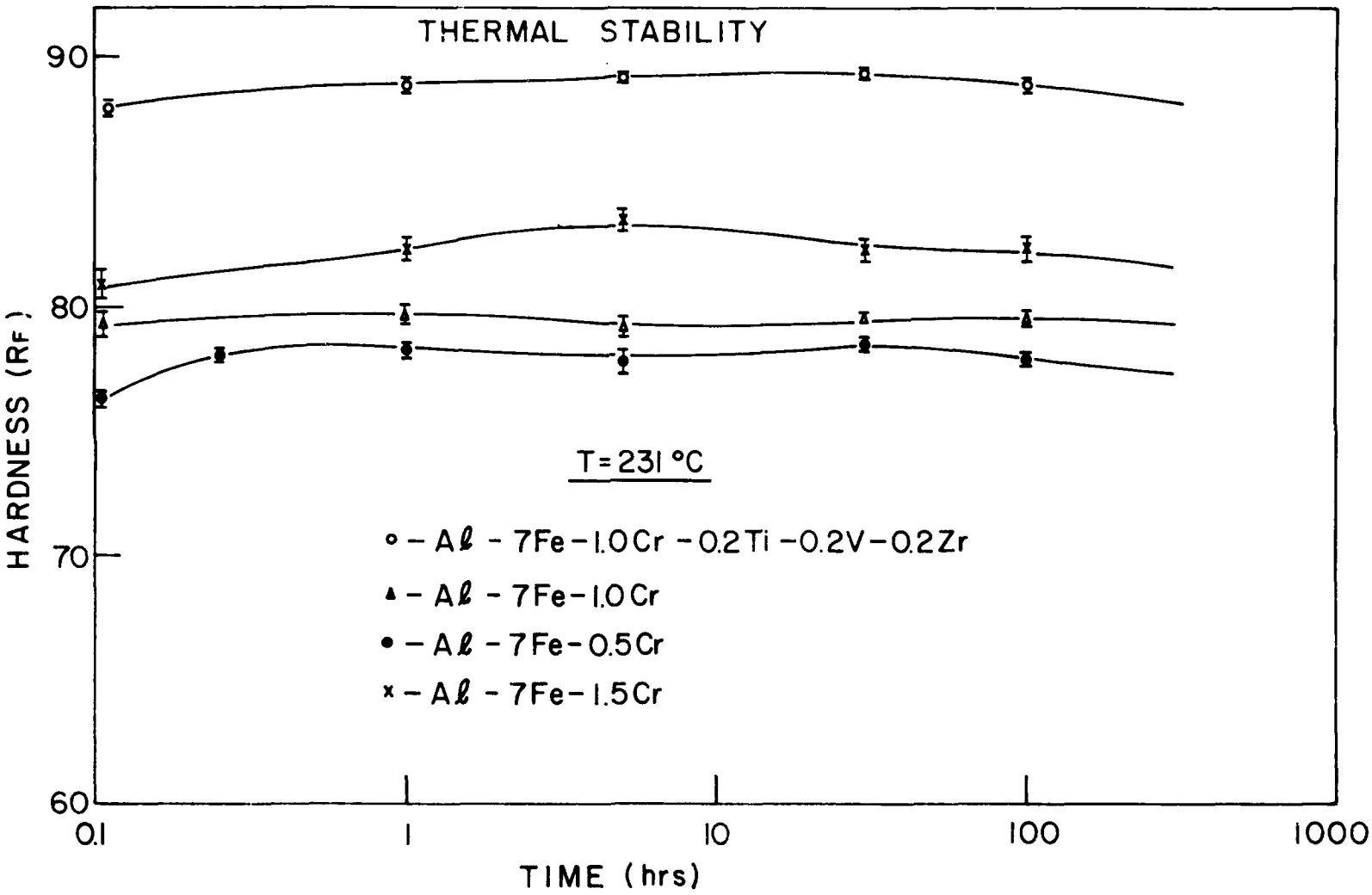
THERMAL STABILITY
90
80
70
60
HARDNESS (RF)
0.1
1
10
100
1000
TIME (hrs)
T=231 °C
o – Aℓ – 7Fe–1.0Cr –0.2Ti –0.2V–0.2Zr
▲ – Aℓ – 7Fe–1.0Cr
• – Aℓ – 7Fe–0.5Cr
x – Aℓ – 7Fe–1.5Cr

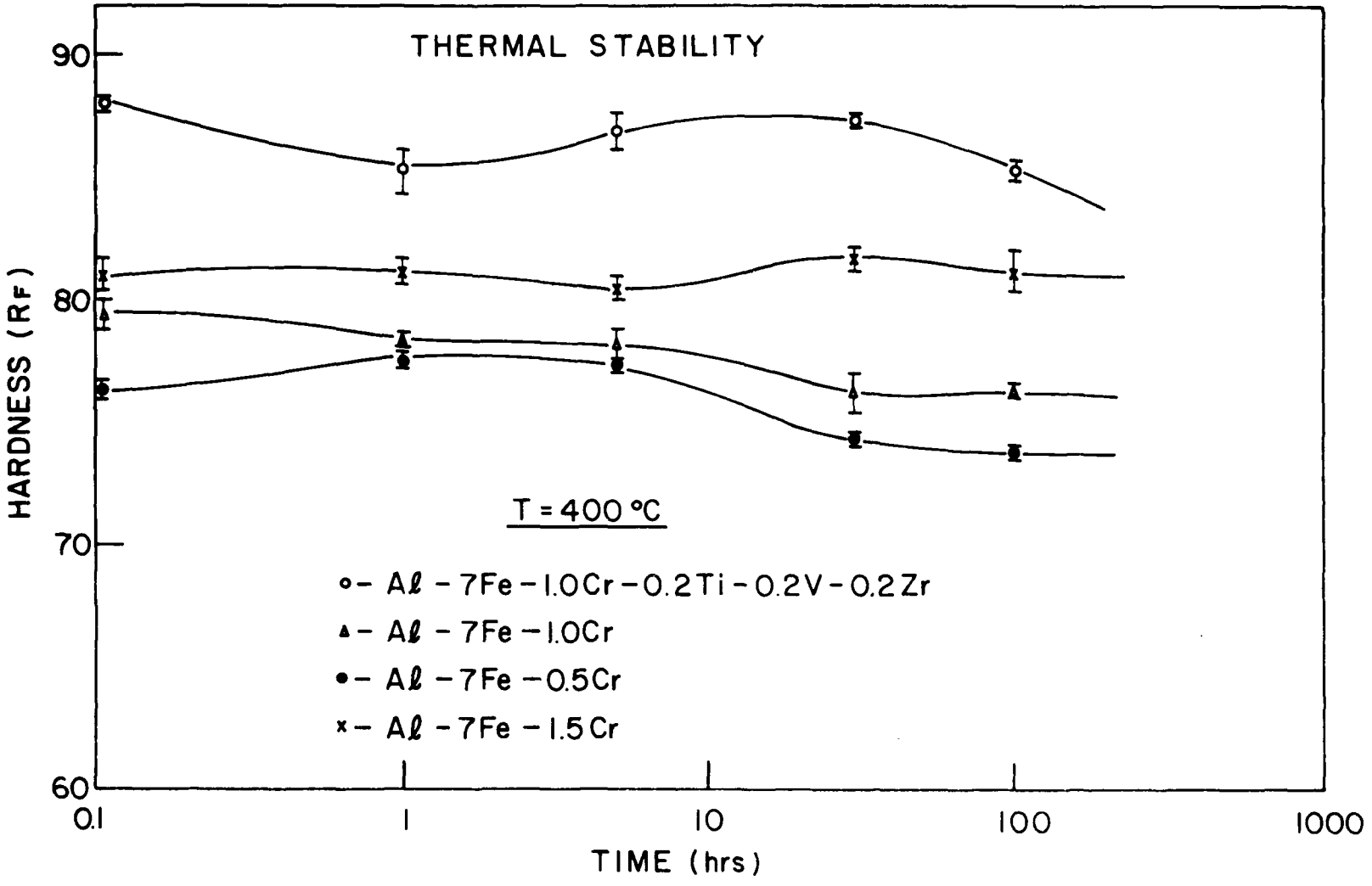
THERMAL STABILITY
HARDNESS (RF)
90
80
70
60
0.1
1
10
100
1000
TIME (hrs)
T = 400 °C
o - Al - 7Fe - 1.0Cr - 0.2Ti - 0.2V - 0.2Zr
▲ - Al - 7Fe - 1.0Cr
● - Al - 7Fe - 0.5Cr
× - Al - 7Fe - 1.5Cr

FIG.4

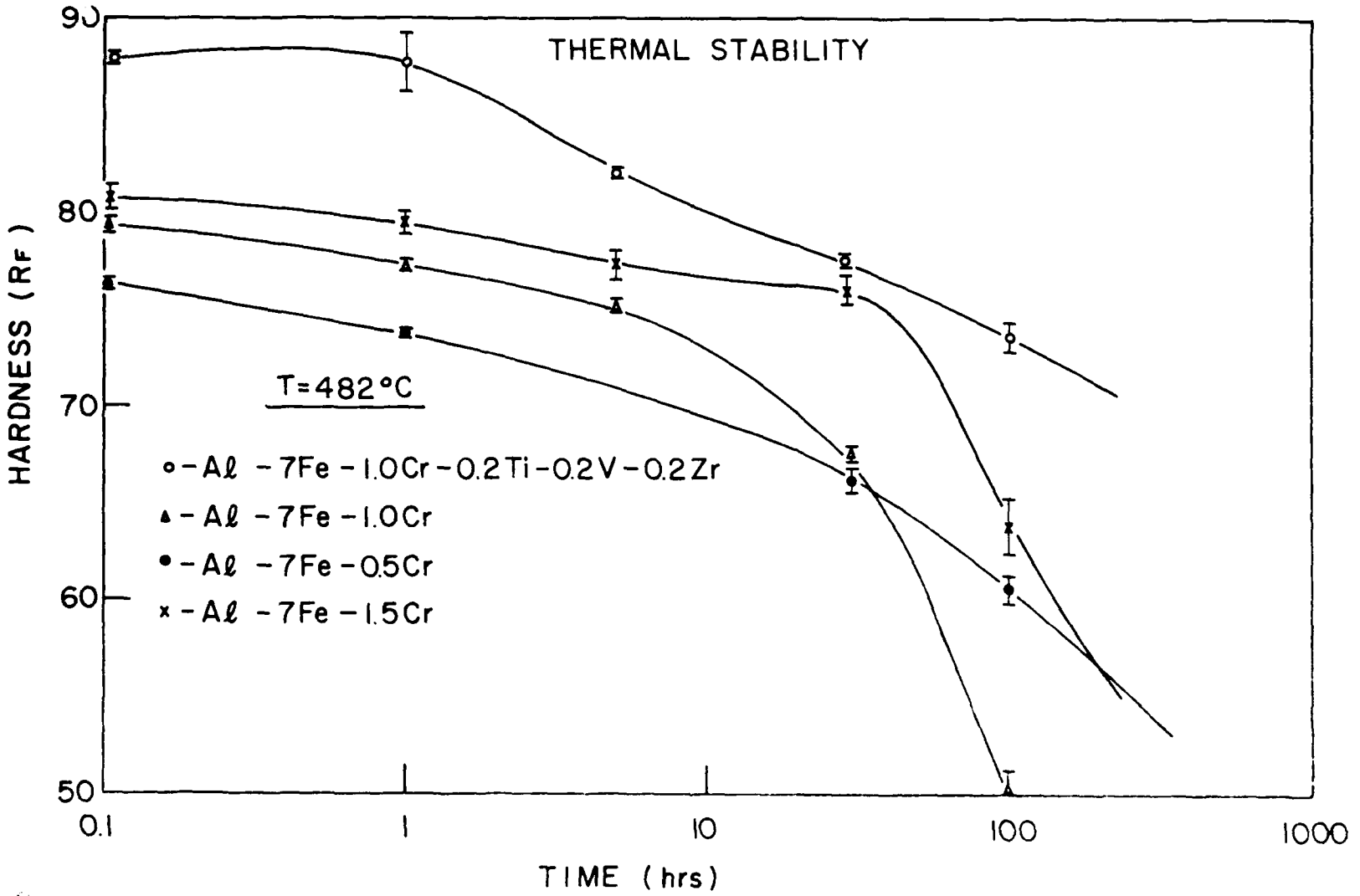
THERMAL STABILITY
HARDNESS (Rf)
90
80
70
60
50
T=482°C
o - Aℓ - 7Fe - 1.0Cr - 0.2Ti - 0.2V - 0.2Zr
▲ - Aℓ - 7Fe - 1.0Cr
● - Aℓ - 7Fe - 0.5Cr
× - Aℓ - 7Fe - 1.5Cr
0.1
1
10
100
1000
TIME (hrs)

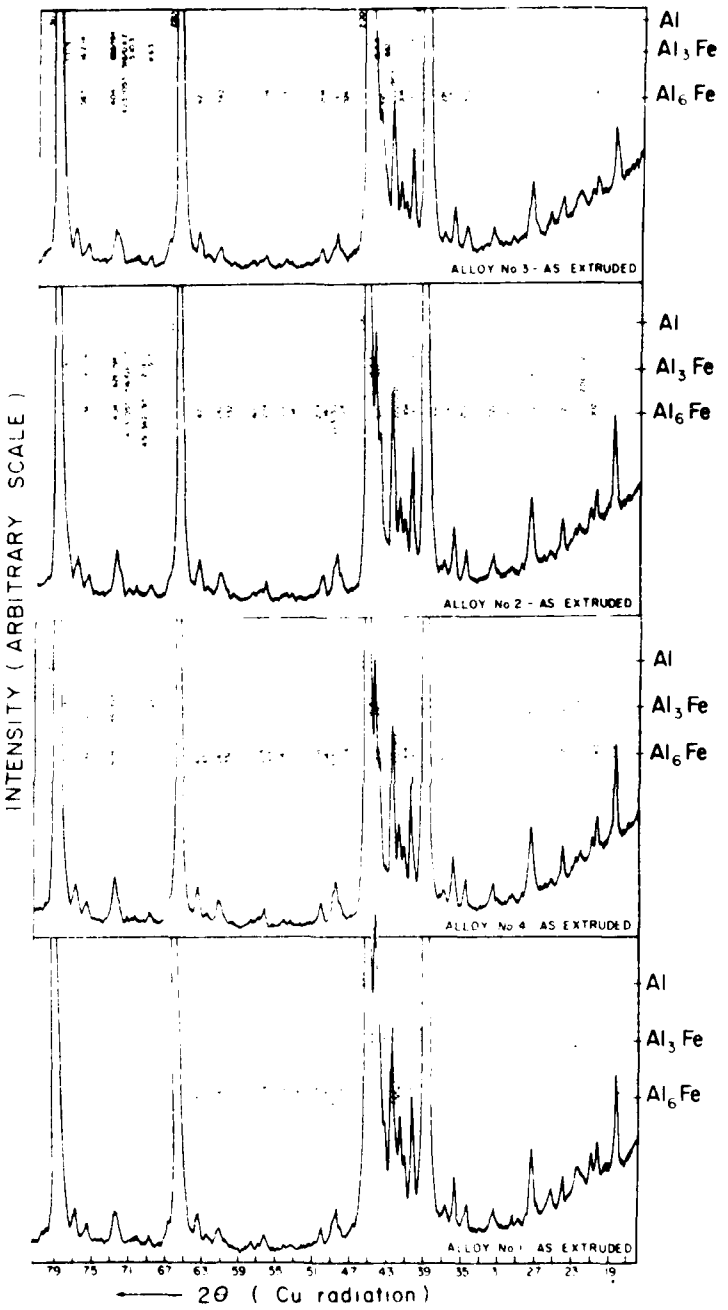
Al
Al3 Fe
Al6 Fe
ALLOY No 3 - AS EXTRUDED
Al
Al3 Fe
Al6 Fe
ALLOY No 2 - AS EXTRUDED
Al
Al3 Fe
Al6 Fe
ALLOY No 4 AS EXTRUDED
Al
Al3 Fe
Al6 Fe
ALLOY No 1 AS EXTRUDED
INTENSITY (ARBITRARY SCALE)
79 75 71 67 63 59 55 51 47 43 39 35 1 27 23 19
2θ (Cu radiation)

Fig. 4

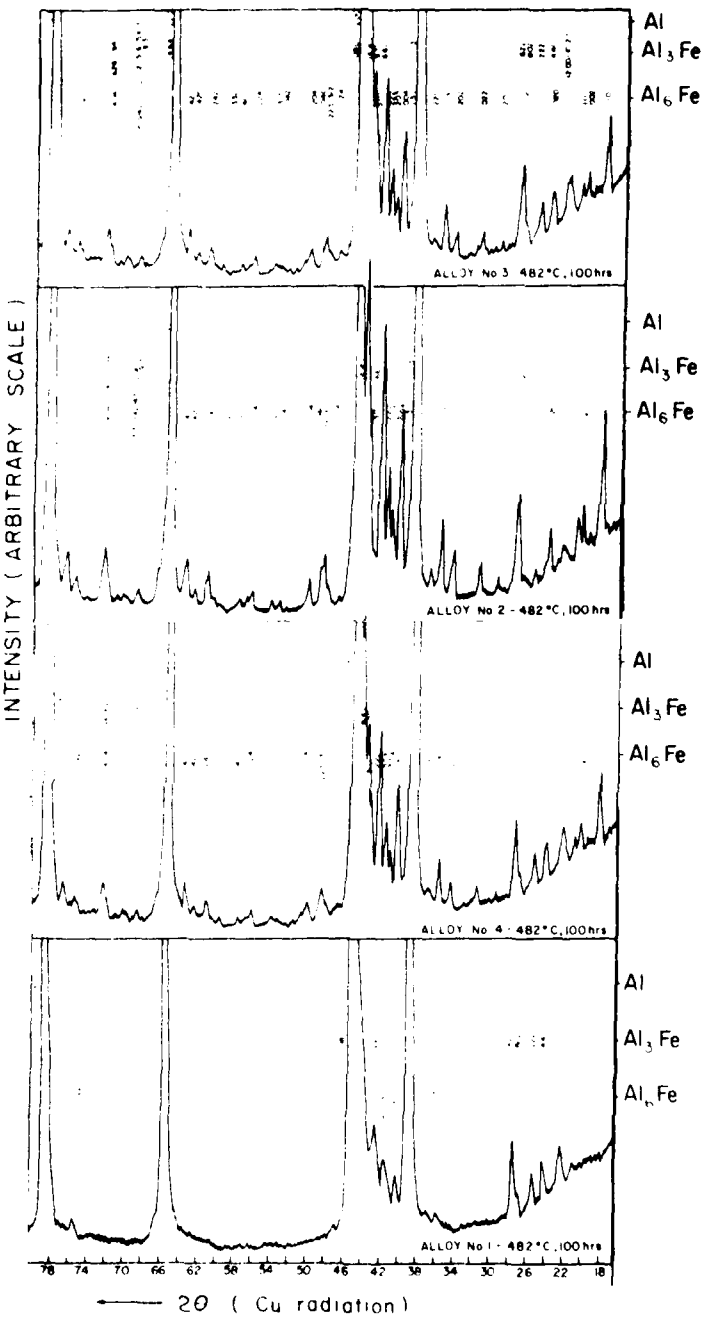
Al
Al3Fe
Al6Fe
ALLOY No 3 482°C, 100hrs
Al
Al3Fe
Al6Fe
ALLOY No 2 - 482°C, 100hrs
Al
Al3Fe
Al6Fe
ALLOY No 4 - 482°C, 100hrs
Al
Al3Fe
Al6Fe
ALLOY No 1 - 482°C, 100hrs
INTENSITY (ARBITRARY SCALE)
78 74 70 66 62 58 54 50 46 42 38 34 30 26 22 18
2θ (Cu radiation)

Fig. 7

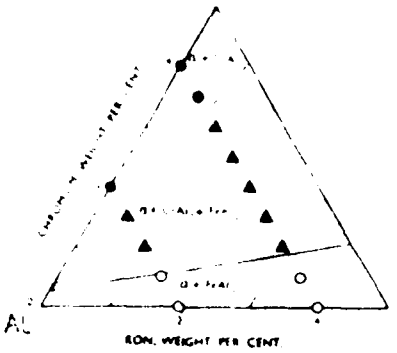

● $\alpha + CrAl_7$; ○ $\alpha + FeAl_3$; ▲ $\alpha + CrAl_7 + FeAl_3$

Fig. 8

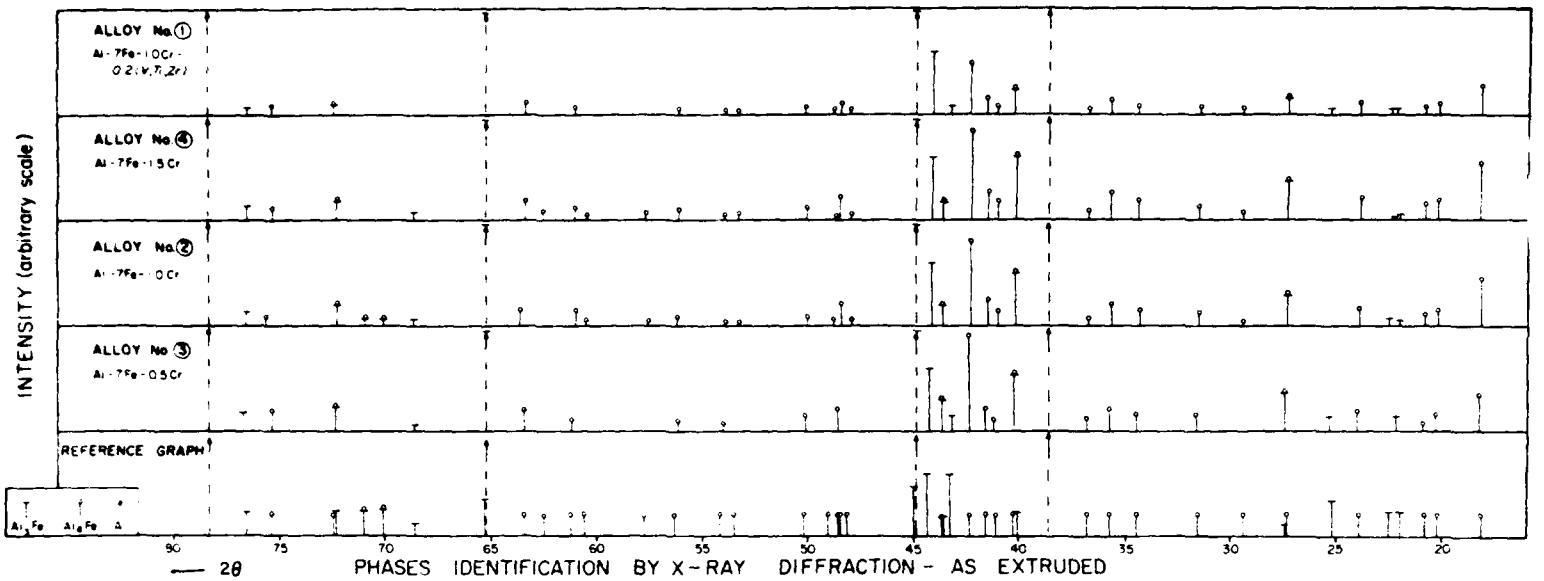

PHASES IDENTIFICATION BY X-RAY DIFFRACTION - AS EXTRUDED

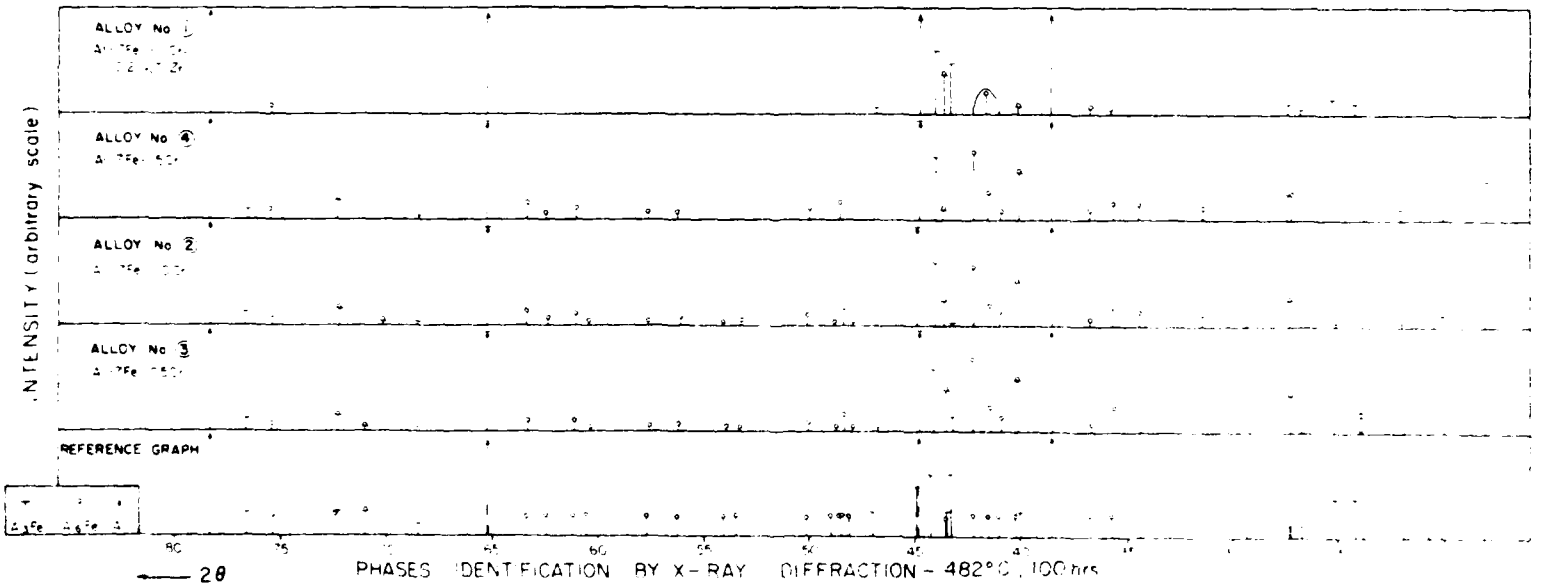

PHASES IDENTIFICATION BY X-RAY DIFFRACTION - 482°C, 100 hrs

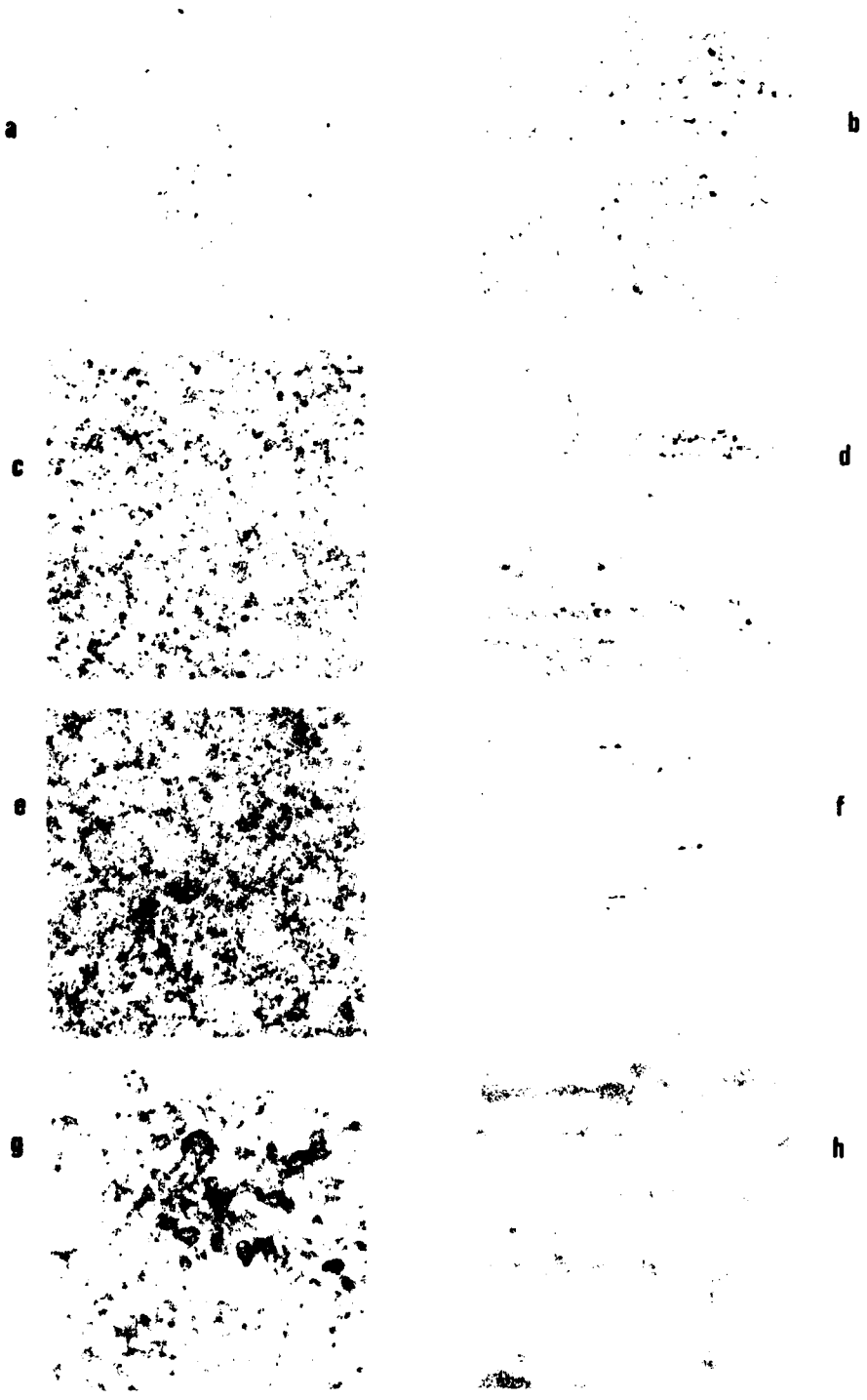

fig.11

a

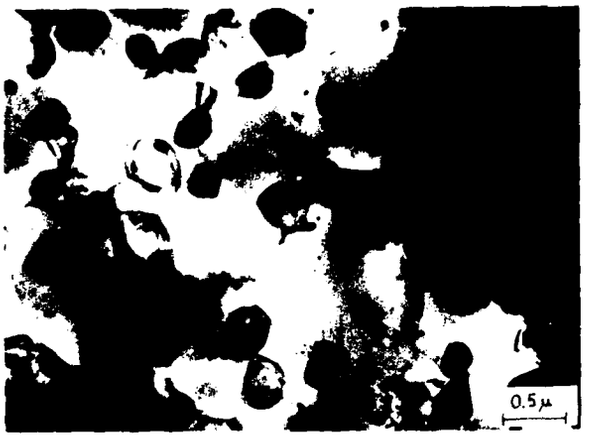

b

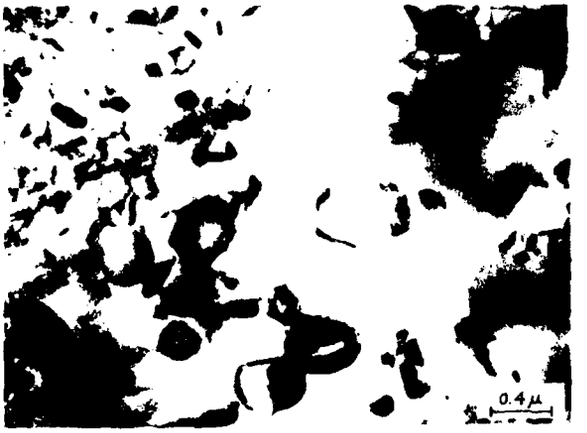

c

d

e

f

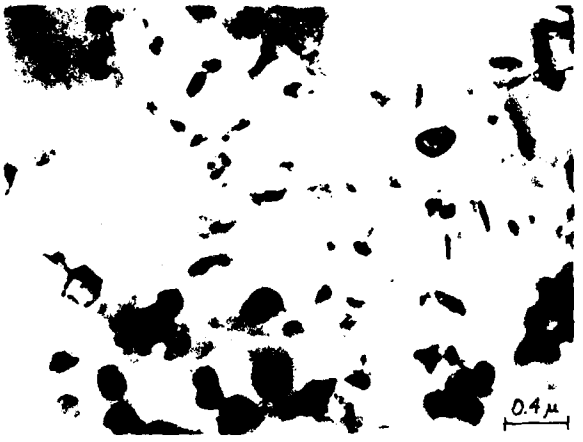

a

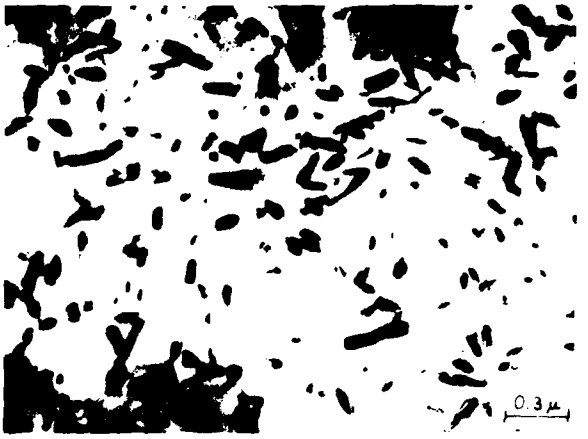

b

c

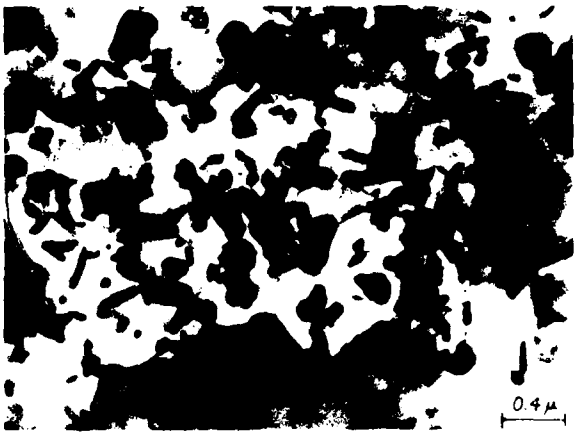

d

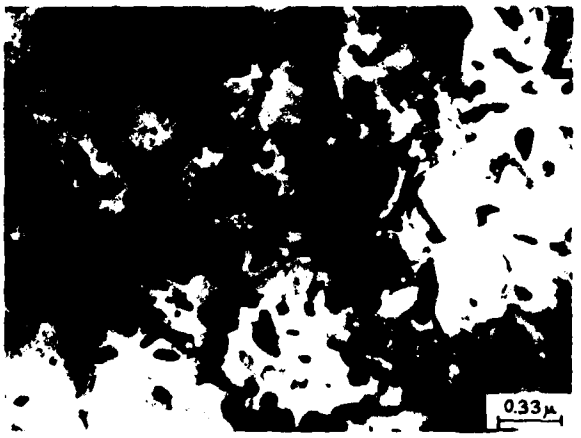

e

f

a

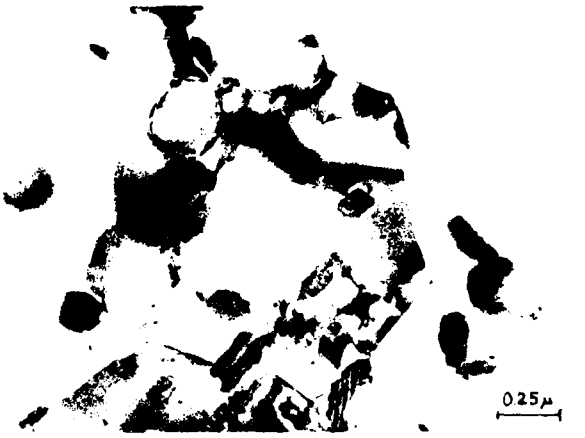

b

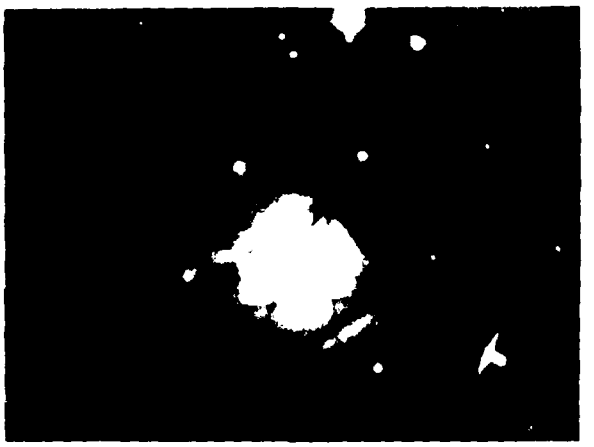

c

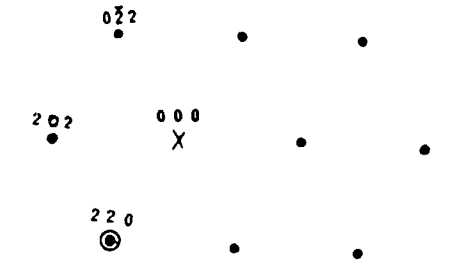

⊙ — Two - beam condition reflection

d

e

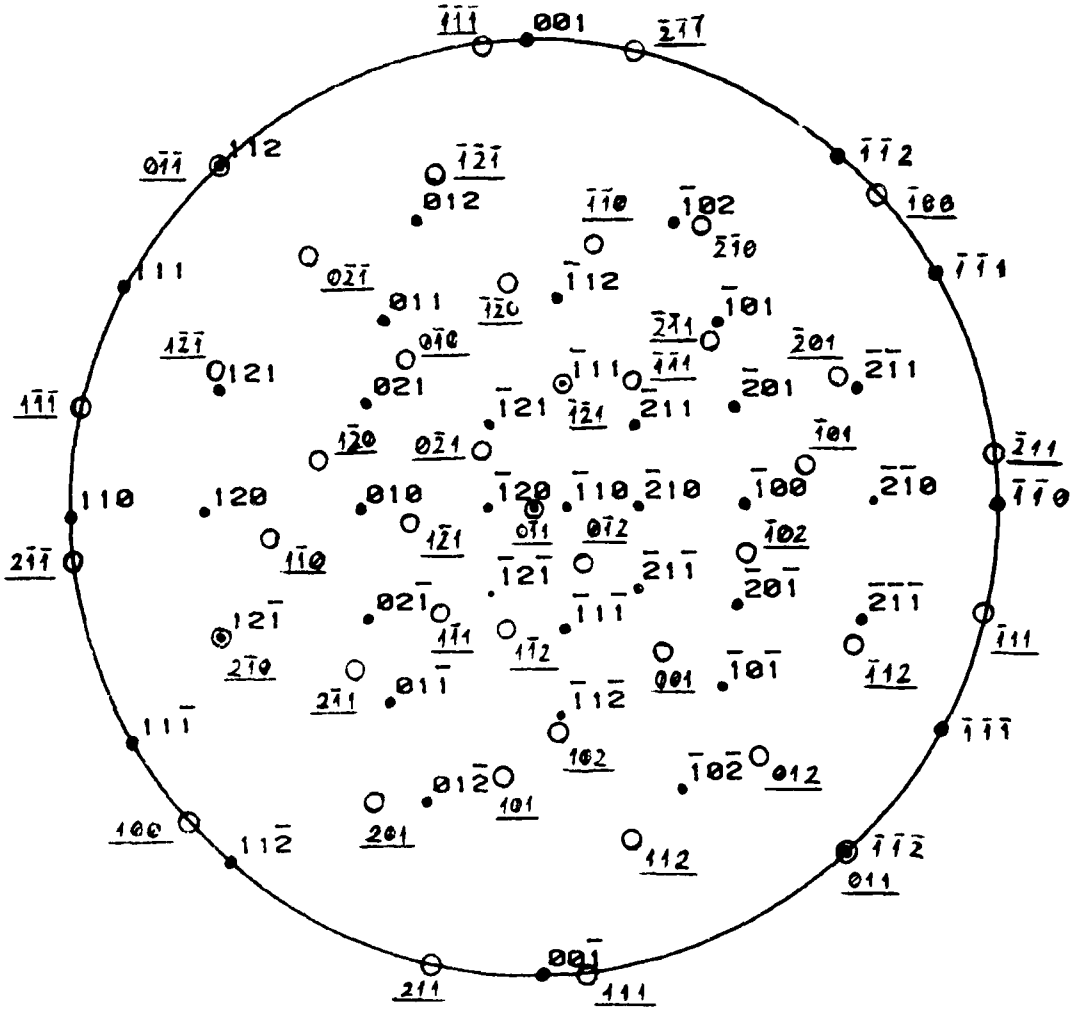

● hkl - Al_6Fe

o hkl - α-Al matrix

fig.15

a

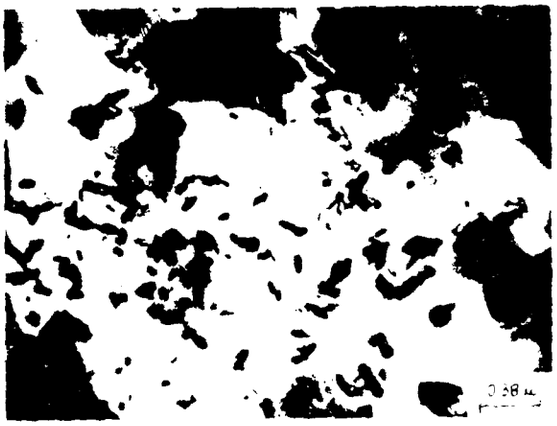

b

c

d

e

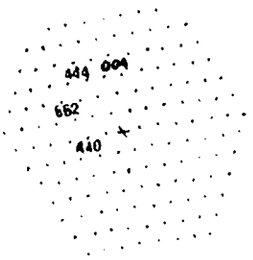

f

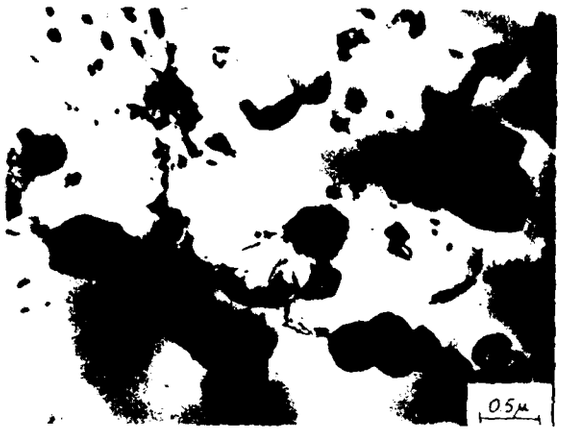

a

b

c

d

e

f

a

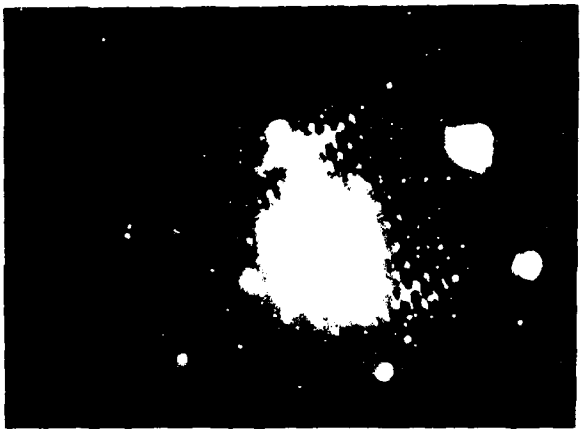

b

c

d

e

f

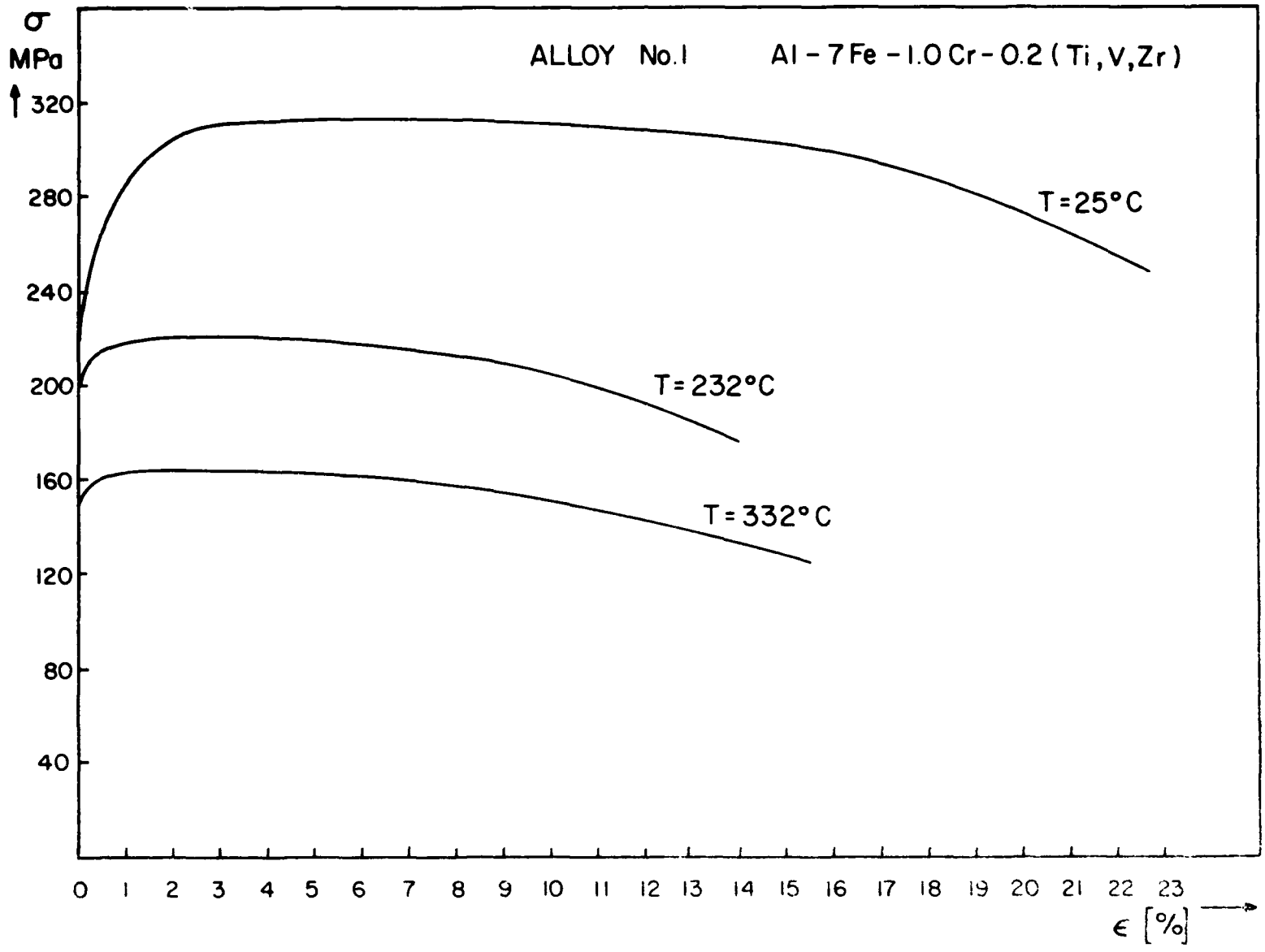
σ
MPa
ALLOY No.1
Al - 7 Fe - 1.0 Cr - 0.2 (Ti, V, Zr)
320
280
240
200
160
120
80
40
T = 25°C
T = 232°C
T = 332°C
0 1 2 3 4 5 6 7 8 9 10 11 12 13 14 15 16 17 18 19 20 21 22 23
ε [%]

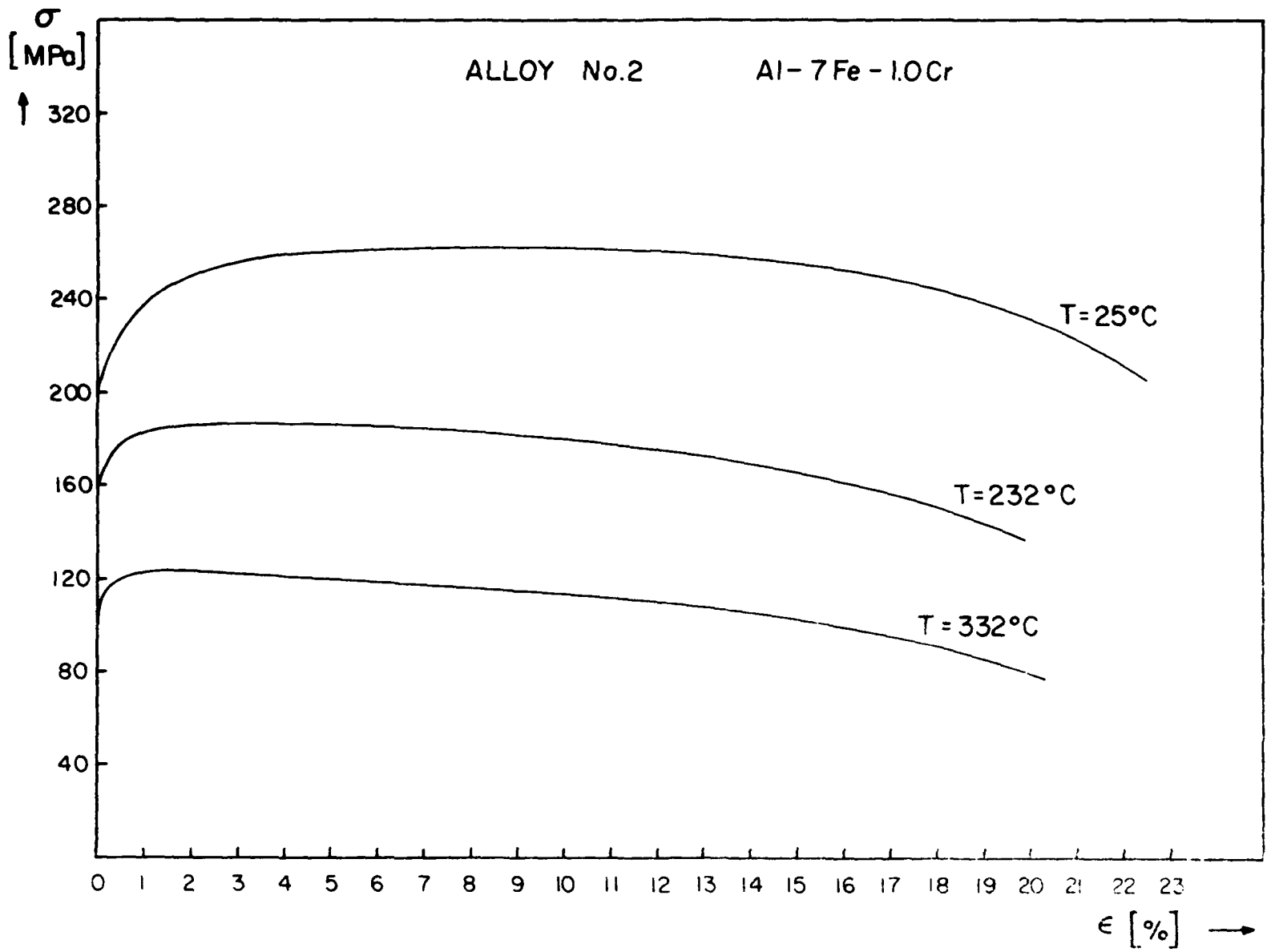
σ
[MPa]
ALLOY No.2
Al – 7 Fe – 1.0 Cr
320
280
240
200
160
120
80
40
T = 25°C
T = 232°C
T = 332°C
0 1 2 3 4 5 6 7 8 9 10 11 12 13 14 15 16 17 18 19 20 21 22 23
ε [%]

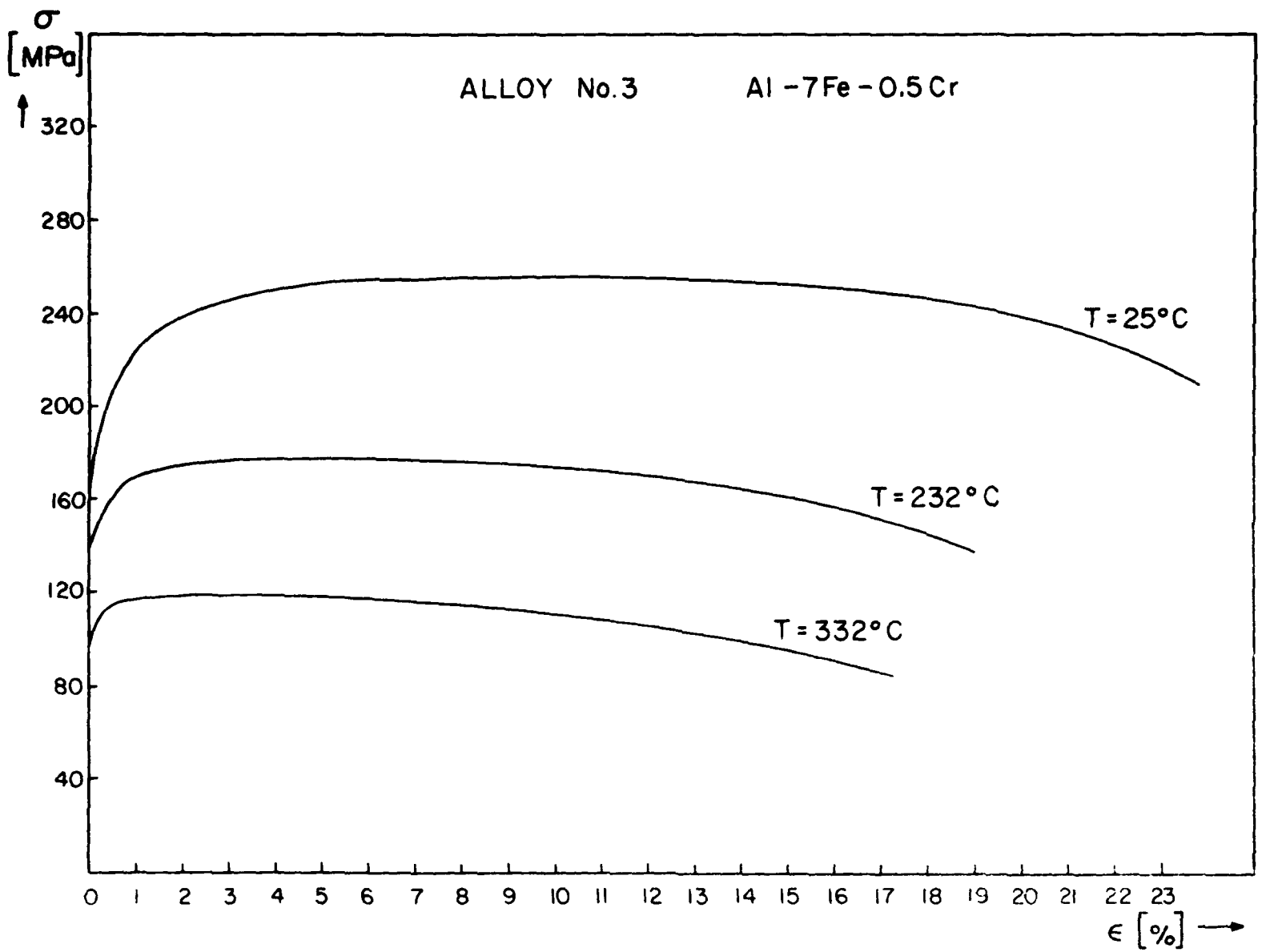
σ
[MPa]
ALLOY No.3
Al - 7Fe - 0.5Cr
320
280
240
200
160
120
80
40
T = 25°C
T = 232°C
T = 332°C
0 1 2 3 4 5 6 7 8 9 10 11 12 13 14 15 16 17 18 19 20 21 22 23
ε [%]

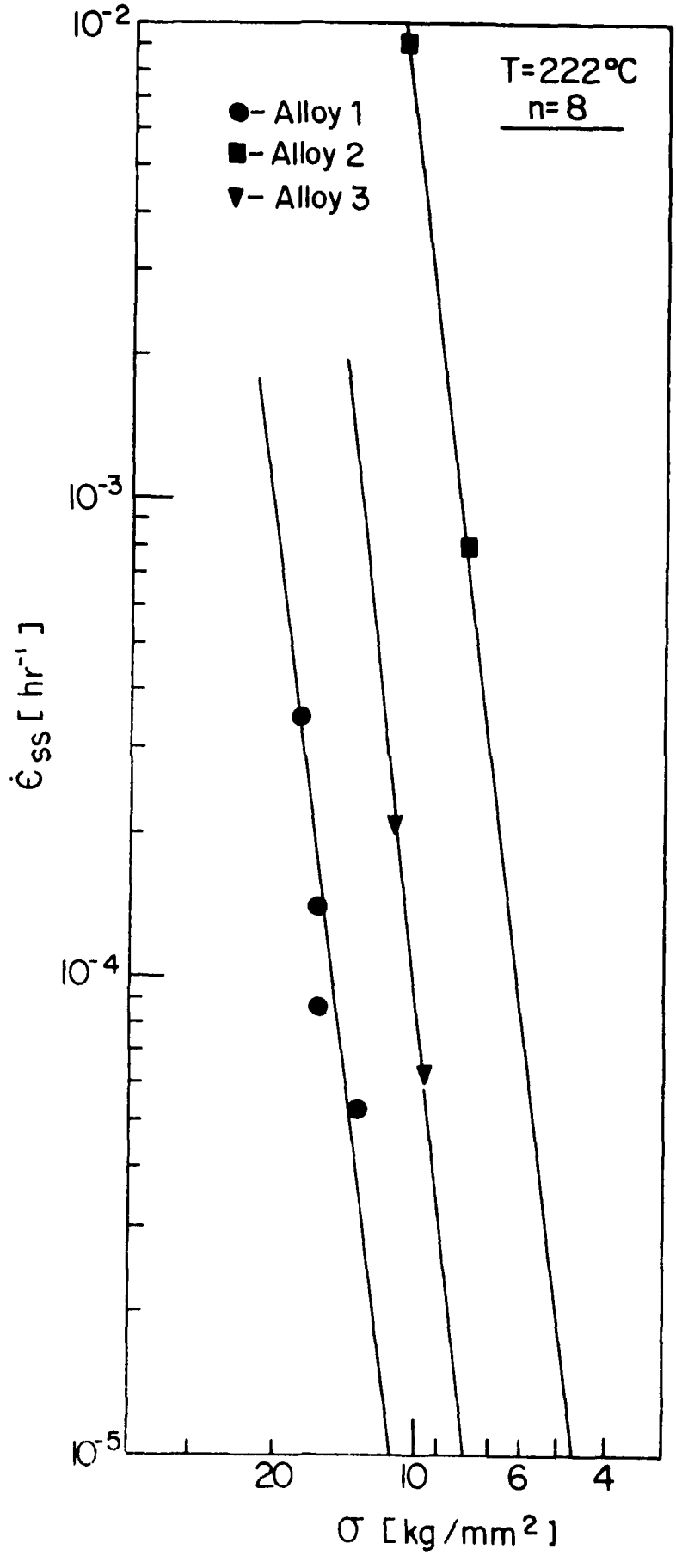
T=222°C
n=8
●- Alloy 1
■- Alloy 2
▼- Alloy 3
10^{-2}
10^{-3}
10^{-4}
10^{-5}
$\dot{\epsilon}_{ss}$ [hr^{-1}]
20
10
6
4
σ [kg/mm^2]

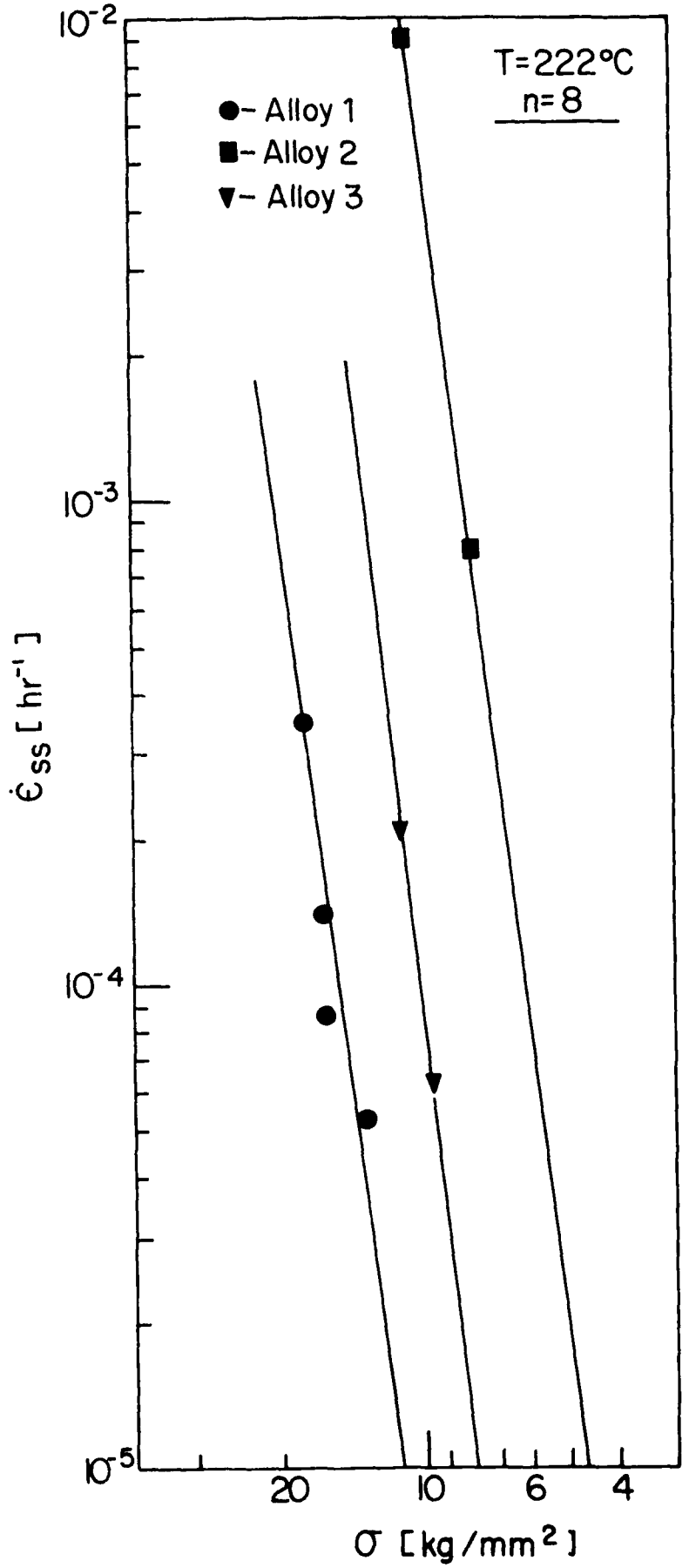
T=222°C
n=8
●- Alloy 1
■- Alloy 2
▼- Alloy 3
10^{-2}
10^{-3}
10^{-4}
10^{-5}
$\dot{\epsilon}_{ss}$ [hr^{-1}]
20
10
6
4
σ [kg/mm^2]

fig.22

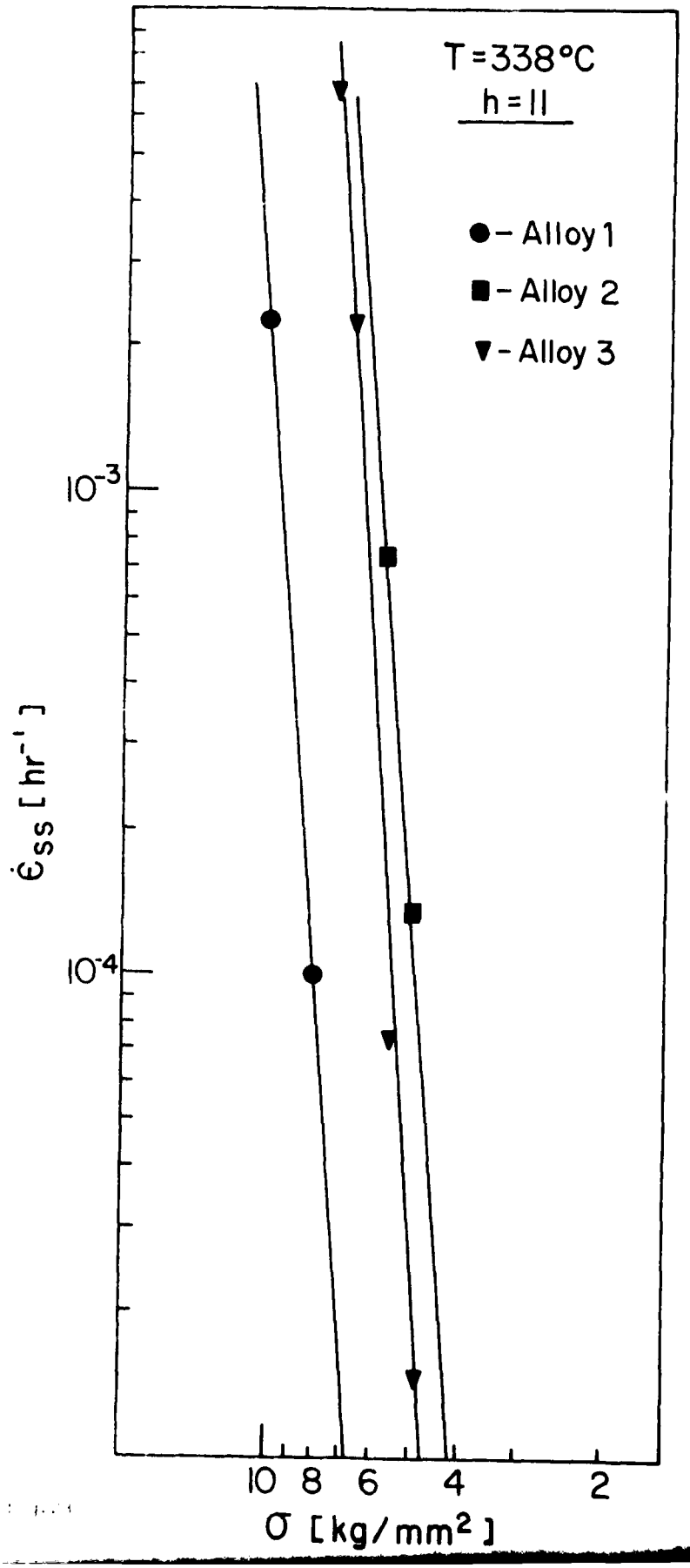
T=338°C
h=11
●- Alloy 1
■- Alloy 2
▼- Alloy 3
10^{-3}
10^{-4}
$\dot{\epsilon}_{ss}$ [hr^{-1}]
10 8 6 4 2
σ [kg/mm^2]

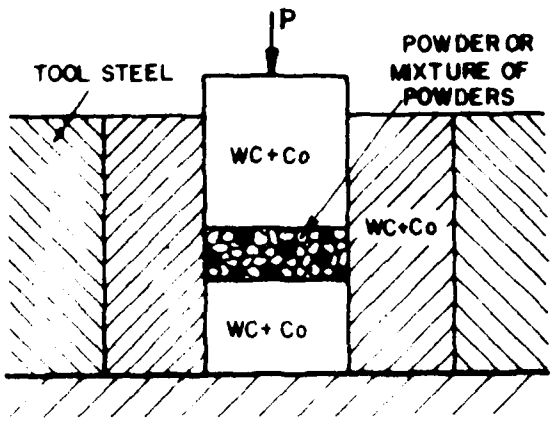

fig.A1

FIG. A2

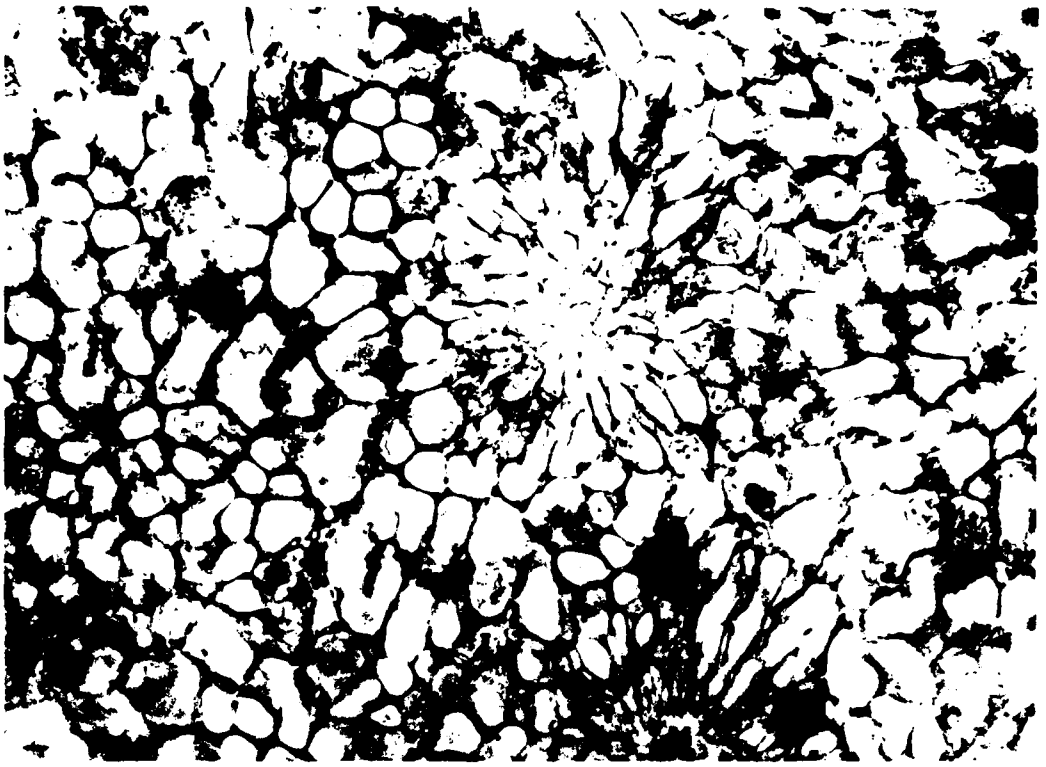

Fig.A3

Fig.A4

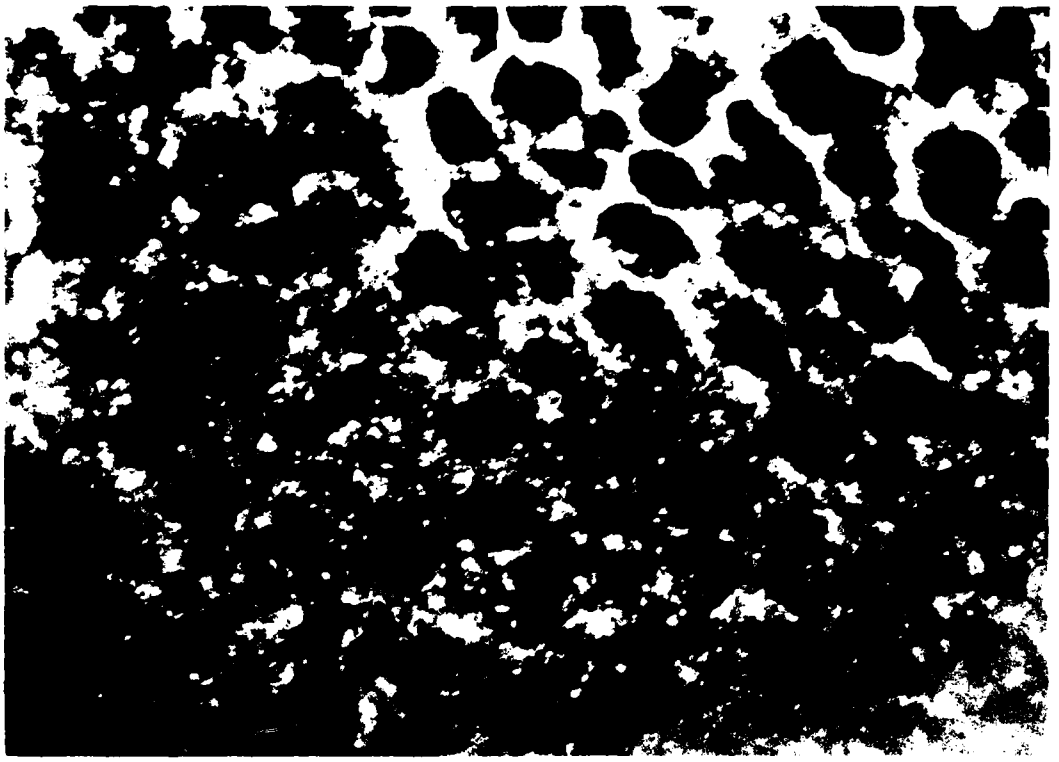

Fig. A5

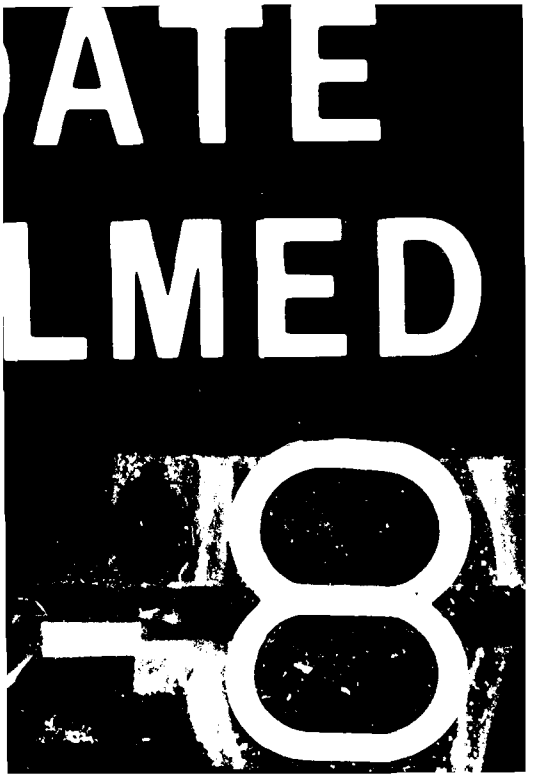
ATE
LMED
8